RESEARCH ON MONOLITHIC MILLIMETER-WAVE DEVICES

Final Report

by

STEVEN E. SCHWARZ

August 1, 1985 to July 31, 1989

for

U. S. Army Research Office

Contract DAAG29-85-K-0182

ELECTRONICS RESEARCH LABORATORY

College of Engineering
University of California, Berkeley
94720

REPORT DOCUMENTATION PAGE

Form Approved
OMB No. 0704-0188

1a. REPORT SECURITY CLASSIFICATION Unclassified	1b. RESTRICTIVE MARKINGS
2a. SECURITY CLASSIFICATION AUTHORITY	3. DISTRIBUTION / AVAILABILITY OF REPORT Approved for public release; distribution unlimited.
2b. DECLASSIFICATION / DOWNGRADING SCHEDULE	
4. PERFORMING ORGANIZATION REPORT NUMBER(S)	5. MONITORING ORGANIZATION REPORT NUMBER(S) ARO 22632.3-EL
6a. NAME OF PERFORMING ORGANIZATION Electronics Research Lab 6b. OFFICE SYMBOL (If applicable) N/A	7a. NAME OF MONITORING ORGANIZATION U.S. Army Research Office
6c. ADDRESS (City, State, and ZIP Code) 253 Cory Hall University of California Berkeley, CA 94720	7b. ADDRESS (City, State, and ZIP Code) P.O. Box 12211 Research Triangle Park, NC 27709-2211
8a. NAME OF FUNDING / SPONSORING ORGANIZATION U.S. Army Research Office 8b. OFFICE SYMBOL (If applicable)	9. PROCUREMENT INSTRUMENT IDENTIFICATION NUMBER DAAG29-85-K-0182
8c. ADDRESS (City, State, and ZIP Code) P.O. Box 12211 Research Triangle Park, NC 27709-2211	10. SOURCE OF FUNDING NUMBERS PROGRAM ELEMENT NO. / PROJECT NO. / TASK NO. / WORK UNIT ACCESSION NO.

11. TITLE (Include Security Classification)

Research on Monolithic Millimeter-Wave Devices

12. PERSONAL AUTHOR(S)

Steven E. Schwarz

13a. TYPE OF REPORT	13b. TIME COVERED	14. DATE OF REPORT (Year, Month, Day)	15. PAGE COUNT
Final	FROM 8/1/85 TO 7/31/89	October 25, 1989	

16. SUPPLEMENTARY NOTATION The view, opinions and/or findings contained in this report are those of the author(s) and should not be construed as an official Department of the Army position, policy, or decision, unless so designated by other documentation.

17. COSATI CODES			18. SUBJECT TERMS (Continue on reverse if necessary and identify by block number)
FIELD	GROUP	SUB-GROUP	millimeter-wave, oscillator, monolithic microwave circuits, Gunn diodes, active device arrays, MMIC

19. ABSTRACT (Continue on reverse if necessary and identify by block number)

The main thrust of this research has been toward improvement of oscillators for planar microwave and millimeter-wave circuits. It seems clear that such oscillators will be important components in future technology. There is a need for local oscillators in receivers; for power oscillators in transmitters; and for arrays of both in scanning radar arrays. In all sorts of oscillators, power drops off as frequency increases. Thus we have been seeking new techniques through which power may be increased. For most applications it is desirable to have low noise as well.

(Continued on next page)

20. DISTRIBUTION / AVAILABILITY OF ABSTRACT ☒ UNCLASSIFIED/UNLIMITED ☐ SAME AS RPT. ☐ DTIC USERS	21. ABSTRACT SECURITY CLASSIFICATION Unclassified
22a. NAME OF RESPONSIBLE INDIVIDUAL	22b. TELEPHONE (Include Area Code) / 22c. OFFICE SYMBOL

We have concentrated most of our attention on transferred-electron (including "Gunn") oscillators. There is a common notion that Gunn oscillators are old-fashioned and that no further improvements are possible. However, the new application in planar circuits creates new needs and constraints that were not present in older waveguide-based work. Furthermore, the advent of MBE makes possible new device structures which were not possible in the past. One such structure is presently being used by us to construct a novel multi-domain Gunn device which is expected to give order-of-magnitude improvement in output power over conventional Gunn devices.

Gunn oscillators have several advantages over MESFET oscillators. One is that unlike MESFETs, which often have very demanding structures with quarter-micron features, Gunn diodes are extremely simple to fabricate. This represents a considerable advantage in terms of cost, yield, and reliability, and makes Gunn diodes exceptionally suitable for use in arrays. Gunn devices also have less noise than MESFET oscillators. As compared with IMPATT oscillators, Gunn devices have less power and smaller frequency range, but have an advantage in terms of noise. The power efficiency of Gunn oscillators is typically rather low, which makes heat dissipation a significant factor.

In our research we have developed the concept of multi-domain Gunn diodes. These are similar to ordinary Gunn diodes, with the difference that several domains move simultaneously from cathode to anode. We have shown that under proper conditions an N-domain diode can have N^2 times the output power of a single-domain diode. This is true even when thermal effects are taken into account. Performance of the multi-domain devices has been studied by means of a partial-differential-equation-solver program written here. We find that the doping profile of the device must be controlled within approximately 20%, in order for the several sections of the device to oscillate in phase. This doping accuracy appears to be well within the capabilities of molecular-beam epitaxy.

The invention of the multi-domain diode is the principal result of our work with Gunn oscillators. It is described in our paper "Multi-domain Gunn Diodes," by J. Tsay, S.E. Schwarz, S. Raman, and J.S. Smith, which has been submitted to Microwave and Optical Technology Letters. We feel that this invention will be important because it will greatly increase the low-noise oscillator power available in planar circuits. It should find use in MMIC communication and radar systems. For example, a 3-domain device should result in an increase in output power by a factor of 9 at 30 GHz, resulting in an estimated output power of 1.8 watts. We are now constructing examples of these new devices and hope to test them within the next six months.

In connection with the work just described, we have also investigated other directions possible with transferred-electron devices. We believe that in MMIC work, "horizontal" devices (i.e., with current flow parallel to the wafer surface) should prove useful. Horizontal devices lend themselves much more readily to the fabrication techniques used in MMICs, resulting in simpler structures. Arrays of devices will be easier to construct than in the case of vertical devices. The geometrical form of horizontal devices would be less ideal; this leads us to suggest going away from transit-time operation, and making use of non-resonant modes of the negative-resistance device. From computation we find that broadband negative resistance can be obtained, suggesting the possibility of widely tunable voltage-tuned oscillators. This is a promising avenue for further work.

We have also studied the design of resonators for planar oscillators. Circuit losses can play a very important role in determining efficiency and output power. In planar circuits, particularly at high frequencies, radiative loss can be a significant component of the loss. We are studying means of designing planar resonators with reduced radiation loss. Electromagnetic computations are being made, supported by experiments with large-scale 1-GHz models. This work is being continued.

A well-known problem in MMIC technology is the difficulty of making adjustments on a circuit once it has been fabricated. We have investigated ways of making such adjustments. Several techniques were demonstrated, ranging from simple mechanical methods to laser photochemical etching.

Another component of our work under this grant has concerned a technique for making measurements on working MMICs. At present it is difficult to find out the current or voltage at a given point in a working circuit, due to the inconvenience of using probes in high-frequency circuits only a millimeter or so in size. We have developed a non-contacting magnetic probe, which couples to currents in the circuit under test like the secondary of a transformer. The probe is about 200 microns in dimension and is made by microfabrication techniques. Extensive design work has been performed using enlarged models at frequencies of 1 GHz and below. Recently microfabricated probes have been built and tested at 33 GHz. Good preliminary results have been obtained. Because of their simplicity, we believe these probes may become important tools for MMIC design. In addition, they can also be used for production testing. Two probes can be used, one for signal injection and another for detection. Such a pair of probes can be moved across a wafer to test individual circuits before the wafer is diced.

Lastly, we have investigated the interesting physical problem of low-frequency oscillations in semi-insulating gallium arsenide. It is found that when a small electric field is applied to this material, low-frequency (audio) current oscillations are observed. This phenomenon has been known for twenty years, but appears never to have been explained. It is thought to be related to the behavior of deep traps in the semi-insulating material. The effect is troublesome in MMICs, where it can add an undesired audio modulation. Furthermore, it is probably related to other undesirable trap-related effects, such as back-gating. We expended some effort in studying the physics of the oscillations in order to determine their cause, but were unable to reach a conclusion. This is a very interesting fundamental problem, and we hope to approach it again at a suitable time.

List of Publications:

(1) C. Zah, D. Kasilingam, J.S. Smith, D. Rutledge, T. Wang, and S.E. Schwarz, "Millimeter Wave Monolithic Schottky Diode Imaging Arrays." Int'l J. Infrared & MM Waves 6, 981-997 (October 1985).

(2) D.F. Williams, S.E. Schwarz, J.H. Sedlacek, and D.J. Ehrlich, "Adjustable Tuning for Planar Millimeter-wave Circuits." Int'l J. Infrared and MM Waves 7, 1729-1746 (November 1986).

(3) D.J. Ehrlich, D.F. Williams, J. Sedlacek, M. Rothschild, and S.E. Schwarz, "High-accuracy Tuning of Planar Millimeter-wave Circuits by Laser Photochemical Etching." IEEE Electron Device Letters EDL-8, 110-12 (March 1987).

(4) S.S. Osofsky and S.E. Schwarz, "A Non-Contacting Probe for Measurements on High-frequency Planar Circuits." Proceedings of 1989 International Microwave Symposium, 823-25.

(5) J. Tsay, S.E. Schwarz, S. Raman, and J.S. Smith, "Multi-domain Gunn Diodes." Submitted to Microwave and Optical Technology Letters.

Research on Monolithic Millimeter-wave Devices

Final Report

I. Introduction

In designing oscillators based on two-terminal devices, it is usually desirable to present the active device with an impedance that results in maximally efficient oscillation at the desired frequency. This requirement conflicts with efforts to increase the output power of the oscillator by increasing the cross-sectional area of the diode. Increasing the area of the diode reduces its impedance, and therefore reduces the impedance that the circuit must present across the diode's terminals. However, circuit losses impose a limit on diode size, because the lower the diode's impedance, the larger the circuit losses become.[1] In this paper we propose multi-domain Gunn diodes, which are in essence series arrays of ordinary Gunn diodes that can be constructed by molecular-beam epitaxy. Such devices would have larger impedance than conventional diodes, leading potentially to large increases in output power.

To illustrate the importance of device impedance, let us consider the circuit shown in Fig. 1. Here a negative-differential-mobility (NDM) device is coupled to a 50-ohm load by means of a transformer. The transformer has reflection coefficient ρ and transmission coefficient τ. Because of the transformer's internal loss mechanisms, a fraction Δ of the power incident on it is lost; that is,

$$|\rho|^2 + |\tau|^2 + \Delta = 1 \qquad (1)$$

Let the power produced by the NDM diode be P_D, and let the powers carried on the line between diode and transformer to the right and left be P_+ and P_- respectively.

Hence $P_D = P_+ - P_-$ and $P_- = |\rho|^2 P_+$. The power P_L delivered to the load is given by $P_L = |\tau|^2 P_+$. Combining these equations we find that the circuit efficiency E_C, defined by $E_C = P_L / P_D$, is given by

$$E_C = 1 - \frac{\Delta}{1 - |\rho|^2} \tag{2}$$

Thus the effect of the circuit loss Δ becomes magnified as $|\rho|^2$ approaches unity. The value of $|\rho|^2$ is determined by G_D and B_D, the optimal load conductance and susceptance of the NDM diode:

$$|\rho|^2 = \frac{(1-x)^2 + (Kx)^2}{(1+x)^2 + (Kx)^2} \tag{3}$$

where $x = G_D Z_0$, $K = B_D / G_D$, and Z_0 is the characteristic impedance of the transmission line. As the diode cross-sectional area is made larger, both G_D and B_D increase in proportion to area, causing $|\rho|^2$ to approach unity and the circuit efficiency to approach zero.

The loss mechanisms just described lead to the well-known "power-frequency limitation," a general limitation of transit-time devices. The power produced by the diode is $P_D = V^2 G_D / 2$, where V, the ac voltage across the diode, is equal to $E_{ac} l$ and l is the length of the diode. We can set $E_{ac} = \alpha F$, where F is the critical electric field. The applied dc field E_{dc} is typically near $(\alpha+1)F$, and the normal range of α is 0.6-2.5 (corresponding to E_{ac} in the range 5,000-11,000 V/cm), with maximum output power occurring near the upper value.[2] Setting $l = v_{sat}/f$, we estimate the ac power of a single-domain diode to be

$$P_D \simeq \frac{1}{2f^2} \left[\alpha^2 F^2 v_{sat}^2 G_D \right] \tag{4}$$

Using equations (2)-(4) and assuming that $\Delta \ll 1$, we find that P_L is maximized when G_D takes the value

$$G_{opt} = \frac{2}{(K^2+1)Z_0\Delta} \tag{5}$$

The resulting maximum output power of the single-domain device is then

$$P_1 = \frac{\alpha^2 F^2 v_{sat}^2}{2f^2(K^2+1)Z_0\Delta} \tag{6}$$

Thus we have the "power-frequency" limitation, according to which output power decreases as f^{-2}. We note that this limitation applies independently of thermal limitations, which will be considered below in Section IV.

In this paper we propose a modified Gunn diode in which several domains simultaneously move from the cathode toward the anode. In this case the total device length L is given by $L = Nv_{sat}/f$, where N is the number of equally-spaced domains. The power-frequency limitation then becomes

$$P_N = \frac{N^2}{2f^2}\left[\frac{\alpha^2 F^2 v_{sat}^2}{(K^2+1)Z_0\Delta}\right] \tag{7}$$

Thus in the absence of heat limitations an N-domain diode should be able to deliver N^2 times as much power at a given frequency as a conventional single-domain diode. The reason for the improvement is that an N-domain diode has N times the impedance of a single-domain diode at the same frequency. Therefore its cross-sectional area can be increased by a factor of N without exceeding the maximum value of conductance the circuit can provide without excessive circuit loss. The volume of the diode and its

power are increased by N^2.

Series connection of several Gunn diodes was proposed in 1968 by Thim [3], who noted the potential relaxation of the power-frequency limitation. By stacking several wafers of 40-micron thickness, he was able to demonstrate series operation at 1.3 and 2.5 GHz. The idea was carried further by Slater and Harrison [4], who demonstrated two- and three-domain operation at 2 GHz, using simple "horizontal" diodes (i.e., with current flow parallel to the semiconductor surface). Domains were nucleated by a declivity scratched in the surface of the semiconductor. Their diodes operated in a quenched hybrid mode. In contrast, the device to be considered here is "vertical", and uses highly controllable epitaxial layers, made by molecular beam epitaxy, to nucleate domains. We have found that it is also possible to quench domains by means of other epitaxial layers. This makes it possible to operate the device in the more stable transit-time mode, with efficiency comparable to that of conventional single-domain diodes.

II. Domain Quenching Mechanism

It is clearly possible to simultaneously nucleate a number of domains at arbitrary positions inside a diode by placing doping notches at the desired points. For efficient operation in the transit-time mode it is also necessary that all domains be quenched at approximately the instant that the device voltage reaches minimum. In reference [4] this was accomplished by operating the device in a hybrid mode, in which the device voltage instantaneously decreases to a low value at which all domains are quenched. Operation in the hybrid mode, however, suffers from drawbacks similar to those of the LSA mode, such as poor high-frequency operation and instability. Instead, we propose

to place regions of high doping at positions at which domains are to be quenched. An advantage of this "built-in" domain quenching mechanism is that it removes the heated electrons from the active region very quickly, allowing a new domain to be formed near the cathode. In the LSA and hybrid modes it is necessary to give the carriers time to cool, which places an upper limit on the frequency of operation. The frequency range of the proposed device, however, should be about the same as that of conventional transit-time diodes. A doping profile for the case of a two-mode device is given in Figure 2.

By means of a simplified model we can illustrate the mechanism of domain quenching and estimate the necessary dimensions of the heavily doped regions. Let us model a mature domain, moving at saturation velocity, by a rectangular field distribution, such as the solid curve in Fig. 3(a). This field is bounded by charge concentrations of opposite sign, as shown in Fig. 3(b). When the leading edge of the domain reaches the heavily doped region, the charges at that end of the domain encounter a lower electric field and move more slowly. This allows the charges at the trailing edge of the pulse to catch up. While this is happening, the electric field within the domain (according to Gauss' law) stays nearly constant; thus the voltage drop across the domain decreases toward zero. Since the voltage across the entire diode is not changing, the voltage drop across the domain is replaced by increased field in the doping notches, causing new domains to nucleate.

The velocity of carriers in the drift region is approximately v_{sat}. If we assume that the charges arriving with the domain have little influence on the field in the heavily doped region, the velocity of those charges, once inside that region, will be approximately $v_{slow} = (N_1/N_2)v_{sat}$, where N_1 is the donor concentration in the drift

region and N_2 the donor concentration in the heavily doped region. While the domain is entering the heavily doped region, its length is decreasing at the rate $v_{sat} - v_{slow}$. To ensure that the domain has time to disappear before its leading edge emerges from the heavily doped region, let us set

$$\frac{L_H}{v_{slow}} = \frac{L_D}{v_{sat} - v_{slow}} \tag{8}$$

where L_H is the length of the heavily doped region and L_D is the length of the fully-formed domain. Thus the approximate minimum length of the heavily doped region is

$$L_H = \frac{L_D N_1}{N_2 - N_1} \tag{9}$$

The value of L_D can be estimated by standard methods. (For example, see pp. 661-2 of Ref. [5].) One might expect that making L_H larger than the minimum might add series resistance to the device and thus reduce efficiency. However, for heavily doped layers of any reasonable thickness the additional series resistance is inconsequential. Thus it is not necessary to control the value of L_H with high precision, so long as it is safely above the minimum value.

III. Stabilty of Operation

The performance of the proposed device has been simulated by means of a standard technique.[6] The simulation is one-dimensional and includes field-dependent mobility and diffusion coefficients.[7] In its present form the simulation assumes an instantaneous local relationship between mobility and field, and thus omits the effects of finite interband and intraband relaxation times.[8][9][10]. Although such effects are important in the hybrid and LSA modes, they are less important in the transit-time mode. The terminal voltage consists of a dc bias (typically 18V) plus a sinusoidal vol-

tage, the amplitude and frequency of which are adjusted for optimum operation. The admittance and power conversion efficiency of the device are found from the resulting current waveform.

A question of particular interest is whether the several sections of the multi-domain device will really oscillate in phase, with similar amplitude, or whether one domain will grow in size and extinguish the others. In particular, one expects that the device will work best when the sections are most nearly identical, and that operation will be disrupted when the sections are dissimilar. We have investigated this question by means of simulation, in order to determine what degree of dissimilarity can be tolerated. We find that the critical part of the structure in this regard is the nucleation notch. If the resistance of one notch is too large, larger domains will grow in that section, suppressing oscillation in the others. For a two-domain device operating at 10 GHz, we find that oscillation will start and run stably, provided that the two notches differ in doping by less than 20%. At higher frequencies, this requirement becomes less stringent, perhaps because the higher doping level of the drift region makes the difference between the two resistivities less dependent on the notch doping; as a result doping accuracies of 30-40% can sometimes be allowed. An interesting point is that near the optimal operating point, neither the device efficiency nor the circuit efficiency is strongly dependent on E_{ac}; thus a certain amount of imbalance in domain size can be accepted.

The advent of molecular beam epitaxy has provided a means of achieving accurate doping profiles. We note that it is not the absolute value of doping density that is important, but rather its repeatability within a single growth. Nonetheless, we must

address the question of whether MBE is capable of the required accuracy. The doping density in growing epilayers is affected by lattice growth rate, molecular flux of dopant species, and, at very low doping levels, by variations in background impurities. Both lattice growth rate and dopant (silicon) flux are expected to be constant within 5% during a single growth. Ideally, one would wish the maximum impurity doping (which arises mainly from residual carbon in the arsenic) to be less than $3 \cdot 10^{14}$. However, what is actually required is not that impurity doping be this small, but rather that it not vary by more than this in the course of a single growth. For instance, if the actual impurity level were $6 \cdot 10^{14}$, we need only require that its variations be less than 50%. We do not have direct evidence that background variations are less than this, and suspect that obtaining such measurements would be difficult. However, there seems no reason to suspect *ab initio* that such variations would exist.

Typical simulation results are given in Table 1. The devices being simulated are those of Fig. 2, the notch concentrations n_1 and n_2, as well as the positions x_1 and x_2 being adjustable. Here R_0 is the device's low-field resistance and η is its internal energy conversion efficiency. Column (a) of the table represents an "ideal" two-domain device with identical doping notches and no temperature gradients, while column (b) represents a similar device in which there is a 20% difference in the doping of the two notches. The output power is almost unaffected by this change. Column (c) represents a device with ideal doping but with temperature gradients, as will be discussed in the following section. The evolution of the electric field for these three cases is shown in Figure 4. The fourth column of the table shows the properties of a conventional single-domain device of the same area for comparison. For both single-domain and two-domain devices we find a smaller ratio of device susceptance to

conductance than did Copeland, presumably because we have chosen an nl product about twice as large. Simulations with larger numbers of domains also show stable operation and give corresponding results.

By means of simulation it is also possible to verify the required thickness of the heavily-doped domain-killing layers between the sections. Figure 5 shows the minimum length of this layer for devices similar to that of Fig. 2, but with heavily-doped layers of various concentrations. (By minimum we mean the thickness below which stable two-domain operation is not obtained with only dc voltage applied. Slightly smaller thicknesses are sufficient in ac operation.) The estimate of equation (7) is shown for comparison. (The value of L_D used in (7) is the one observed in simulation.) Agreement is good considering the simplicity of the estimate, and it appears that (7) can be used as a convenient lower bound.

IV. Thermal Limitations

Even if the sections of the device are fabricated identically, operation will still become unbalanced if the sections differ in temperature. Such effects can be simulated by including the temperature dependence of mobility and diffusion coefficient.[11] The results indicate that with $N=2$ or $N=3$, stable and efficient operation is obtained when the temperature difference δT between the hottest and coolest places in the device is less than $(\delta T)_N = 50\text{K}$. The performance of a device with this temperature difference is illustrated in (c) of Table 1 and Figure 4. In principle it should be possible to adjust the sizes of the doping notches in order to compensate for thermal effects, and thus achieve more nearly equal domain amplitudes.

Let us adopt a one-dimensional heat flow model, with the device contacted to a heat sink at the anode end. Then

$$\delta T = \frac{gL^2}{2K_S} = \frac{g}{2K_S}\left[\frac{N v_{sat}}{f}\right]^2 < (\delta T)_N \tag{10}$$

where g is the heat power generated per unit volume, L is the total length of the device, and K_S is the heat conductivity. The heat power per unit volume can be written

$$g = \frac{V_{dc} I_{dc}}{NlA} = \frac{(E_{dc} Nl)(nqv_{sat} A)}{NlA} = (\alpha+1) F (nl) qf \tag{11}$$

where A is the cross-sectional area and (nl) is the well-known "nl product." Thus for a given N the dc bias (determined by α) is limited by

$$\frac{F (nl) q v_{sat}^2 N^2}{2K_S} \frac{\alpha+1}{f} \leq (\delta T)_N \tag{12}$$

The value of α is also limited by the form of the J-E curve and possible breakdown to a maximum of about 2.5 [2]. For frequencies above f_N, given by

$$f_N = \frac{1.75 F (nl) q v_{sat}^2 N^2}{K_S (\delta T)_N} \tag{13}$$

the value of α allowed by (12) exceeds 2.5, and hence the thermal limit has no effect; thus for $f \geq f_N$, the available power is simply given by (7), with $\alpha=2.5$. However, for $f < f_N$, alpha must be reduced to satisfy (12), resulting in

$$P_N = \frac{N^2 F^2 v_{sat}^2}{2(K^2+1) Z_o \Delta} \left[\frac{3.5}{f_N} - \frac{1}{f}\right]^2 \qquad (f \leq f_N) \tag{14}$$

As typical values for GaAs we may take $v_{sat} = 10^7$ cm/sec, $F = 3\times10^3$ V/cm, $K = 3$, $\Delta = 0.03$, $Z_0 = 50\ \Omega$, $(ni) = 10^{16}$ m^{-2}, $K_S = 50$ W/meter·deg.[2][5] The power available as a function of frequency is then as shown in Figure 6, for several values of N. The power of a single-domain diode is limited by (6) and by its own maximum allowable temperature rise $(\delta T)_1$. Because the latter is larger than $(\delta T)_N$, f_1 is below the frequency range of interest, and P_1, which is given by (6) with $\alpha = 2.5$, is as shown in the figure. We find that $f_2 = 13.4$ GHz, $f_3 = 30.2$ GHz, $f_4 = 53.6$ GHz, etc. For $f \geq f_N$, the power of the N-domain diode is N^2 times as large as that of a single-domain diode. For example, a 3-domain diode should be able to produce 1.8 W at 30.2 GHz, as compared with 0.2 W for a single-domain diode at the same frequency.

V. Conclusions

In principle, an N-domain diode can provide output power substantially larger than that of a single-domain diode. In favorable frequency ranges the improvement is on the order of N^2. The multi-domain device is in essence a series array of diodes, but will take up no more space than a single diode, and will be unaffected by parasitics such as would appear between elements of a side-by-side array. Thermal rise places limits on operation, but substantial improvements should be possible even within these limits.

Series connections of Gunn diodes have been considered in the past, but have not been successful, because of the difficulty of fabricating the devices accurately enough. In order to achieve stable multi-domain operation, the doping profile must be repeated, from section to section of the device, with high accuracy. New techniques of fabrication, such as molecular beam epitaxy, have improved the available accuracy of doping profiles, and it now appears that the necessary precision can be achieved. The problem of low impedance also arises with other transit-time devices such as IMPATT diodes, and the approach of using several in series may be useful in those cases as well.

Acknowledgements

This research has been supported by the U.S. Army Research Office under grant DAAG29-85-K-0182 and by the Joint Services Electronics Program.

References

[1] H. Kroemer, Proc. IEEE **54**, 1980-81 (1966)

[2] J.A. Copeland, "Theoretical Study of a Gunn Diode in a Resonant Circuit." IEEE Trans. Electron Devices ED-14, 55-58 (Feb. 1967).

[3] H.W. Thim, "Series-Connected Bulk GaAs Amplifiers and Oscillators." Proc. IEEE 56, 1244 (1968)

[4] M. Slater and R.I. Harrison, "An Investigation of Multiple Domain Gunn Effect Oscillators." IEEE Trans. Electron Devices ED-23, 560-67 (June 1976).

[5] S.M. Sze, *Physics of Semiconductor Devices*, 2nd edition. Wiley-Interscience (1981).

[6] M.R. Lakshminarayana and L.D. Partain, "Numerical Simulation and Measurement of Gunn Device Dynamic Microwave Characteristics". IEEE Trans Electron Devices ED-27, pp 546-552 (1980).

[7] H.L. Grubin, "Large-signal Computer Simulations of the Contact, Circuit, and Bias Dependence of X-band Transferred Electron Oscillators." IEEE Trans Electron Devices ED-25, 511-19 (May 1978).

[8] H. Kromer, "Hot-electron Relaxation Effects in Devices." Solid State Electronics 21, 61-67 (1978).

[9] D. Jones and H.D. Rees, "Electron-relaxation Effects in Transferred- electron Devices Revealed by New Simulation Method." Electronics Letters 8, 363-4 (1972).

[10] R. Bosch and H.W. Thim, "Computer Simulation of Transferred Electron Devices Using the Displaced Maxwellian Approach." IEEE Trans. Electron Devices ED-21, 16-24 (January 1974).

[11] K.R. Freeman and G.S. Hobson, "The Vf Relation of CW Gunn Effect Devices." IEEE Trans. Electron Devices ED-19, 62-70 (1972).

Figure Captions

Fig. 1.

Fig. 2. Doping profile of 10-GHz two-domain device. At the points marked "Ohmic contact" the boundary condition $E = 0$ is applied. Each heavily-doped layer has width 1.4 μm and the width of each doping notch is 0.4 μm. The width of the buffer section between heavily doped layer and doping notch is 0.2 μm. Values of x_1, x sub 2 ,n_1, and n_2 are given in Table 1.

Fig. 3. Electric field (a) and charge density (b) of domain entering heavily-doped region. The solid curves represent the domain before it has entered; the dashed curves after it has entered.

Fig. 4. Electric field versus position at several times in a cycle, for the devices of Table 1, columns (a), (b), and (c).

Fig. 5. Minimum L_H for devices similar to that of Fig. 2, as obtained from simulation. The estimate of equation (7) is shown for comparison.

Fig. 6. Theoretical output power of multi-domain devices vs. frequency, assuming parameter values as mentioned in the text. The power of a single-domain device is shown for comparison.

Table 1

Device Data And Simulation Results

	(a)	(b)	(c)	(d)
length (μm)	$x_1 = 10.5$	$x_1 = 10.5$	$x_1 = 9.5$	$x_1 = 10.5$
	$x_2 = 21.0$	$x_2 = 21.0$	$x_2 = 19.0$	
R_0 (ohms)	7.90	7.79	7.15	3.95
freq (GHz)	10	10	10	10
area (cm^2)	10^{-4}	10^{-4}	10^{-4}	10^{-4}
n_1 (10^{15} cm^{-3})	1.0	1.0	1.0	1.0
n_2 (10^{15} cm^{-3})	1.0	1.2	1.0	
η (%)	7.12	7.05	6.89	7.44
G_D (mho)	-5.3×10^{-3}	-5.26×10^{-3}	-4.76×10^{-3}	-1.10×10^{-2}
$\left\lfloor G_D \times R_0 \right\rfloor^{-1}$	23.9	24.4	29.4	23.0
B_D (mho)	1.01×10^{-2}	1.11×10^{-2}	9.30×10^{-3}	2.06×10^{-2}
$\left\lfloor \frac{B_D}{G_D} \right\rfloor$	1.91	2.11	1.95	1.87
power (W)	0.468	0.464	0.421	0.243

Device (a): identical sections, no temperature gradient

Device (b): 20% doping notch variation, no temperature gradient

Device (c): identical sections, 50° temperature difference

Device (d): single-domain device

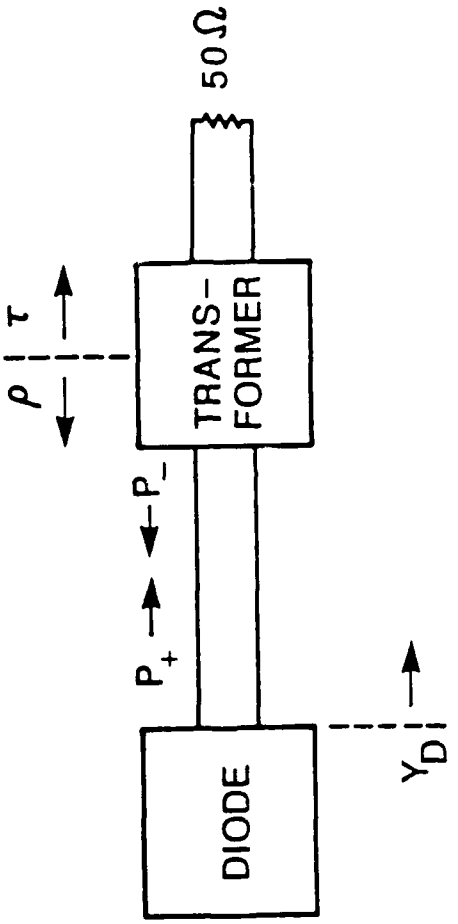

FIG. 1

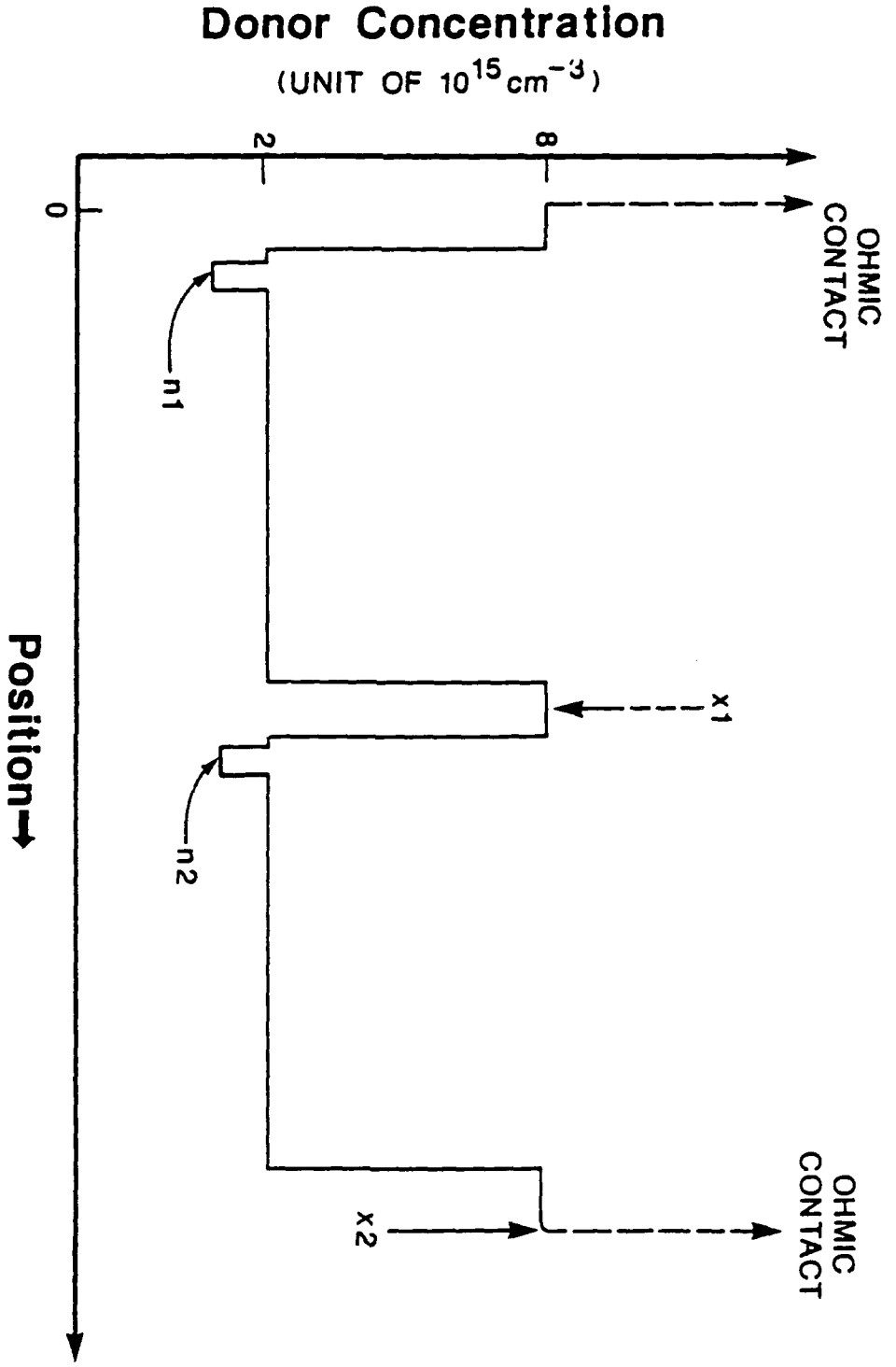
Donor Concentration
(UNIT OF $10^{15}cm^{-3}$)
2
8
0
OHMIC CONTACT
n1
x1
n2
x2
OHMIC CONTACT
Position

FIG. 2

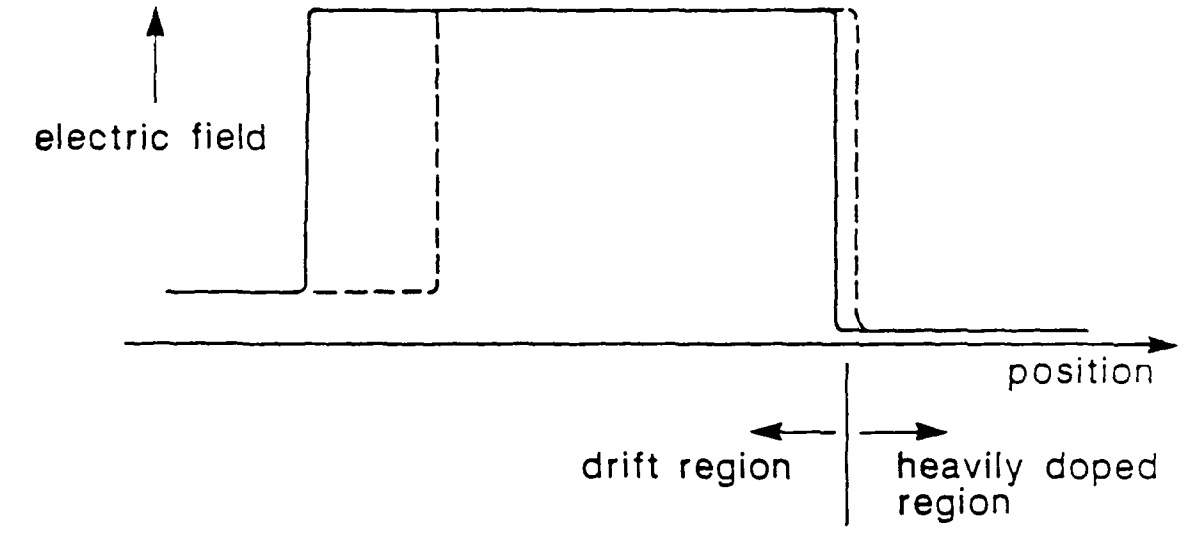
electric field
position
drift region
heavily doped region

(a)

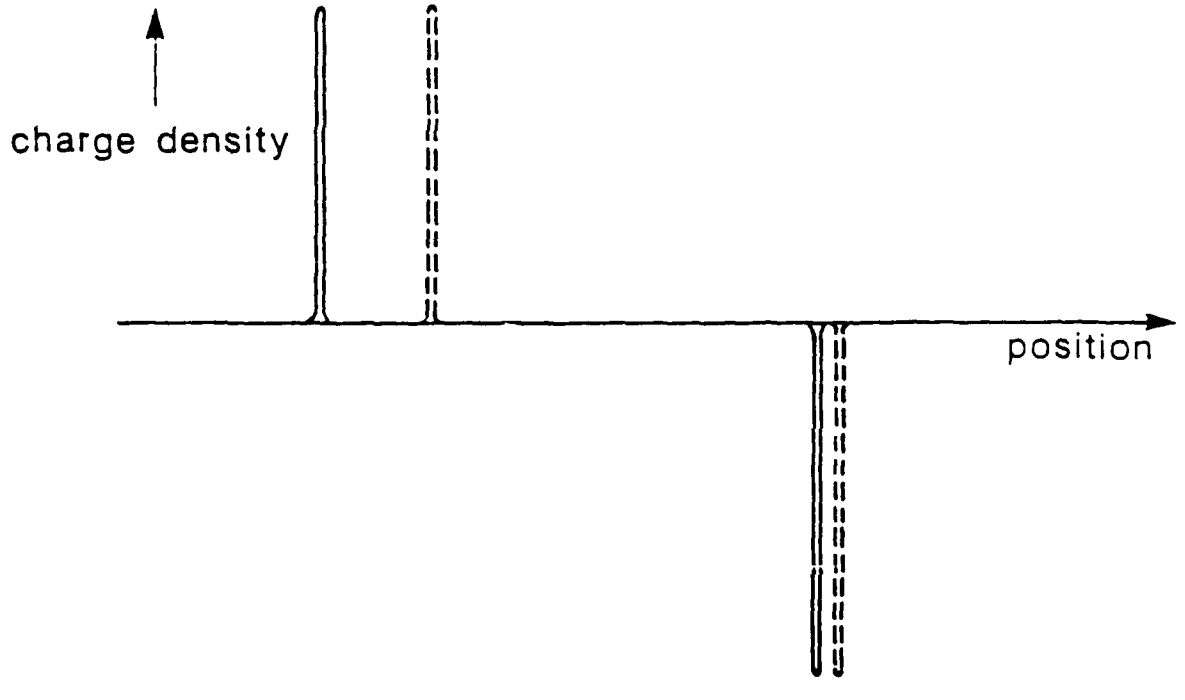
charge density
position

(b)

FIG 3

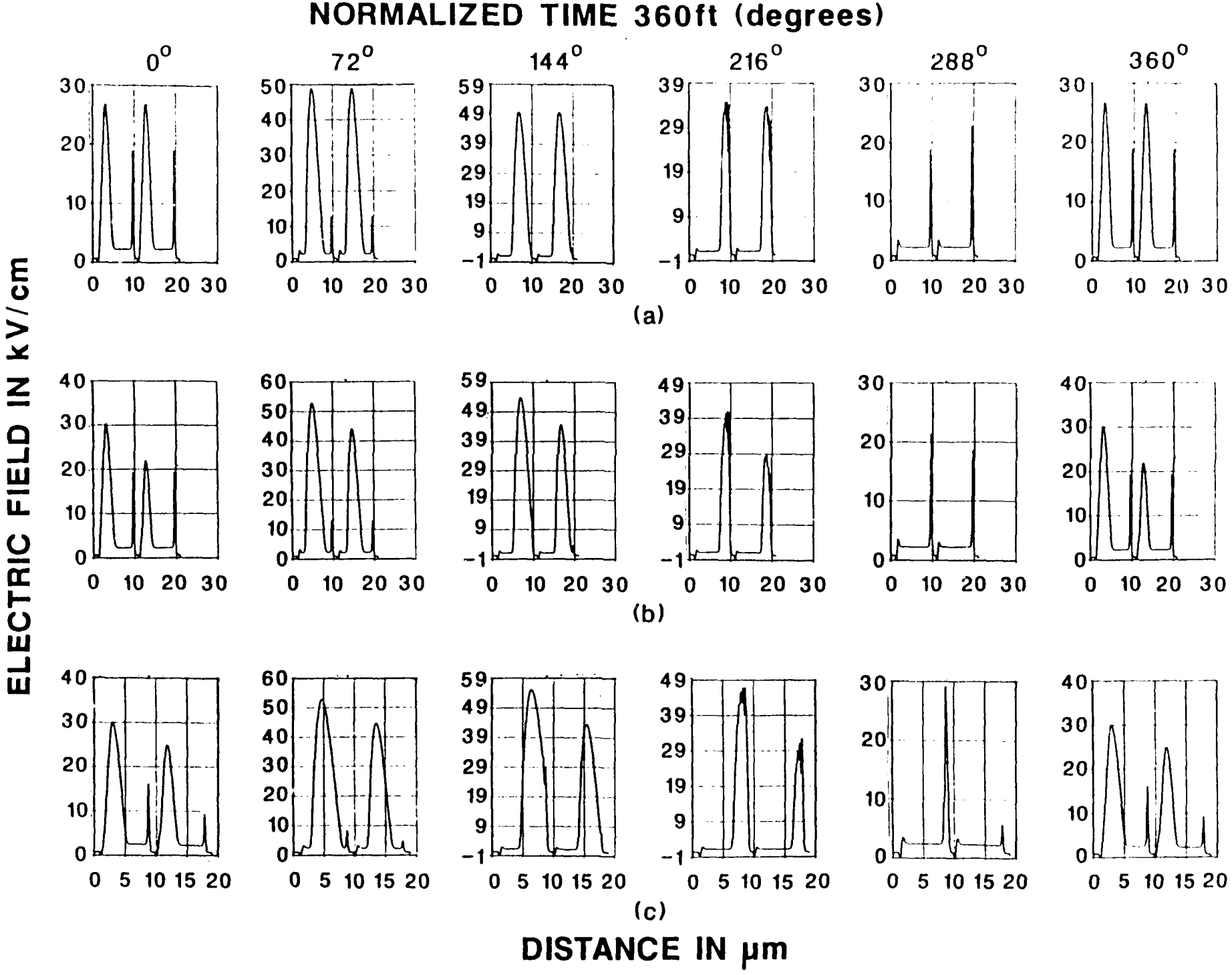
NORMALIZED TIME 360ft (degrees)
0°
72°
144°
216°
288°
360°
(a)
(b)
(c)
ELECTRIC FIELD IN kV/cm
DISTANCE IN μm

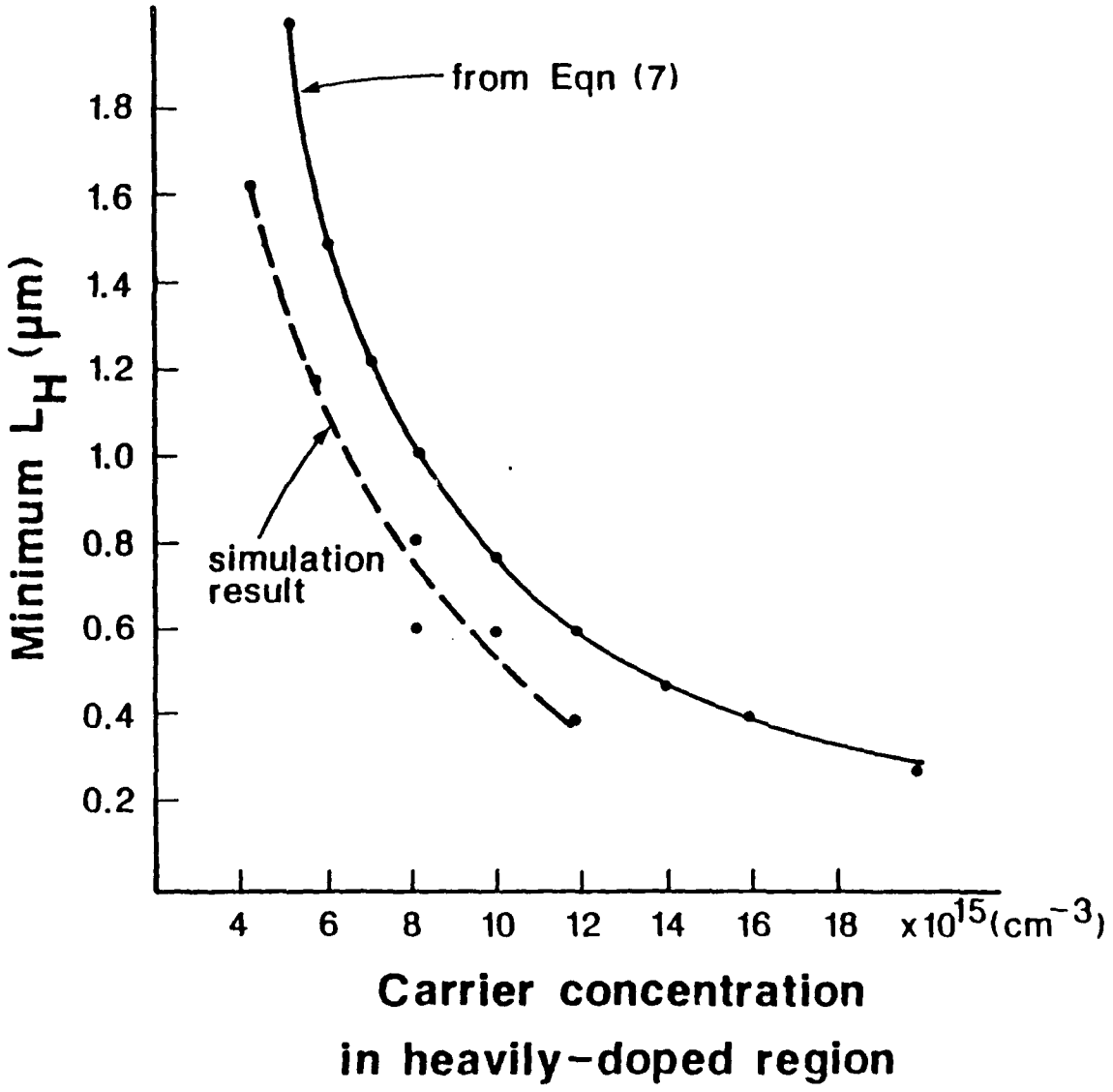
from Eqn (7)
simulation result
Minimum L_H (μm)
1.8
1.6
1.4
1.2
1.0
0.8
0.6
0.4
0.2
4
6
8
10
12
14
16
18
x10^{15}(cm^{-3})
Carrier concentration in heavily-doped region

Fig. 5

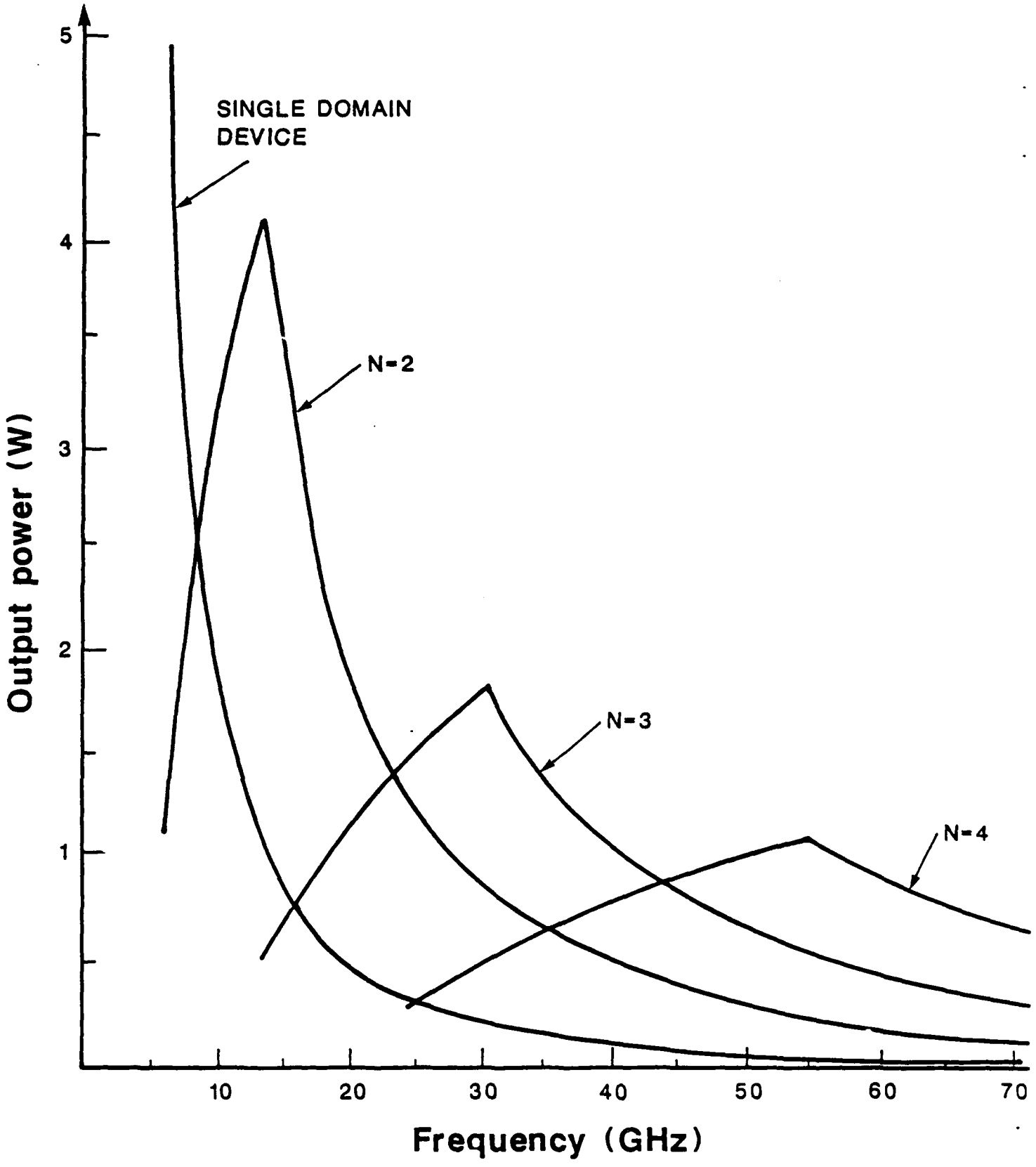
SINGLE DOMAIN
DEVICE
N=2
N=3
N=4
Output power (W)
5
4
3
2
1
10
20
30
40
50
60
70
Frequency (GHz)

FIG. 6

International Journal of Infrared and Millimeter Waves, Vol. 6, No. 10, 1985

MILLIMETER WAVE MONOLITHIC SCHOTTKY DIODE IMAGING ARRAYS

Chung-en Zah, Dayalan Kasilingam, John Steven Smith, and David Rutledge

Division of Enginering and Applied Science
California Institute of Technology
Pasadena, CA 91125

Tai-Chi Wang and Steven E. Schwarz

Department of Electrical Engineering
University of California
Berkeley, CA 94720

Received July 29, 1985

Abstract

Planar Schottky diodes are integrated with bow-tie antennas to form a one-dimensional array. The energy is focused onto the antennas through a silicon lens placed on the back of the gallium-arsenide substrate. A polystyrene cap on the silicon lens reduces the reflection loss. A self-aligning process with proton isolation has been developed to make the planar Schottky diodes with a 1.1-THz zero-bias cutoff frequency. The antenna coupling efficiency and imaging properties of the system are studied by video detection measurements at 94 GHz. As a heterodyne receiver, a double-sideband mixer conversion loss of 11.2 dB and noise temperature of 3770°K have been achieved at a local oscillator frequency of 91 GHz. Of this loss, 6.2 dB is attributed to the optical system and the antenna.

Introduction

Recently Young et al. demonstrated a millimeter-wave plasma imaging system based on an array of bow-tie antennas with microbolometer detectors [1]. Fig. 1 shows the approach. The image is focused first through an objective lens and then through a lens on the back of the substrate onto a linear array of antennas. The signal received by each antenna is detected by the bismuth microbolometer and plotted to form the image. This array is attractive for plasma diagnostics because events occur too quickly for conventional mechanically scanned systems. Imaging arrays are also attractive for imaging in astronomy and military applications when the signal is weak, since they allow more integration time for each element in the array. Microbolometers are not sensitive enough for these applications. However, other sensitive detectors have been developed. Clifton et al have developed an excellent monolithic Schottky diode detector [2], and Wengler et al have demonstrated an extremely sensitive monolithic superconducting tunnel junction (SIS) detector [3]. In this paper we report a monolithic imaging array (see Fig. 2a) for 94 GHz with gallium-arsenide Schottky-diode detectors (see Fig. 2c and 2d). Each array has nine elements. The optical system consists of a TPX objective lens and a silicon lens on the back of the gallium-arsenide wafer (see Fig. 2b).

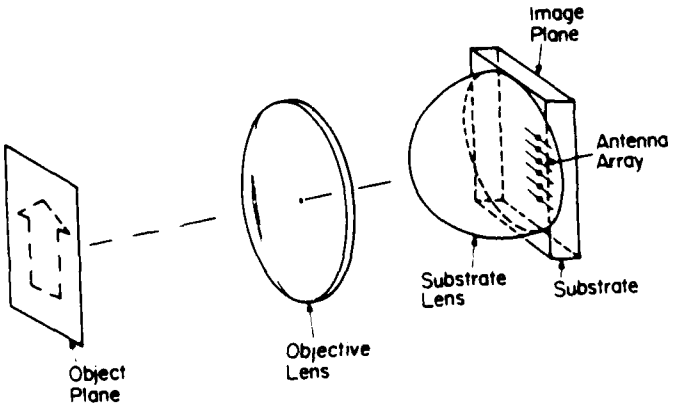

Fig. 1 Imaging antenna array.

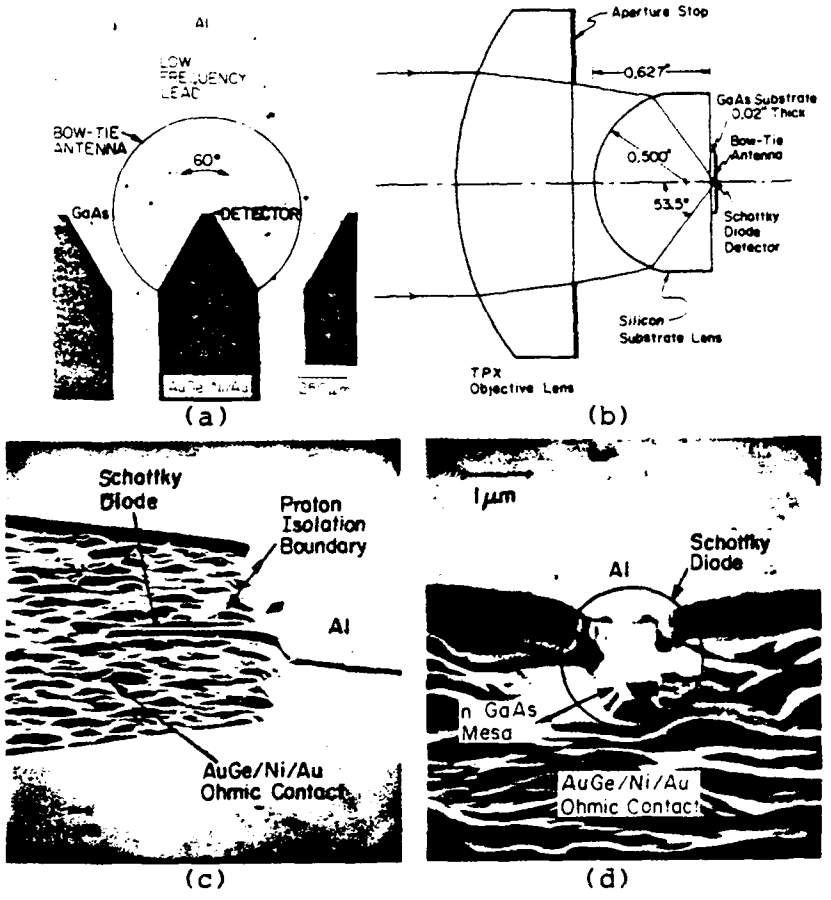

Fig. 2 Imaging antenna array for 94GHz. The antennas are bow-ties (a), and the Schottky-diode detectors are at the apex of each bow. The arrays contain nine antennas and detectors 0.75mm apart. The optical system is shown in (b), and the diode is shown from the side in (c) and from the end in (d).

Fabrication

The Schottky diode is the critical element of the array. Fig. 3 shows the structure. The Schottky electrode is a narrow stripe 0.8 μm wide by 6 μm long (see Fig. 2c and 2d). This gives a high

periphery-to-area ratio for low series resistance. The diodes were made on top of a semi-insulating GaAs substrate. All the epitaxial layers and the aluminum were grown in situ by molecular beam epitaxy (MBE). The bottom n^+ layer is approximately 1.4 μm thick with a doping concentration of $3x10^{18}$ cm^{-3}. Its thickness is chosen so that it can be completely converted into a semi-insulating layer by proton bombardment with an energy of 300 keV. The n layer is 0.1 μm thick with a doping concentration of 10^{17} cm^{-3}. It is designed to be depleted at zero bias to reduce the series resistance due to an undepleted n layer. The doping concentration of the n layer is chosen to achieve a relatively small tunnel current at room temperature and a small series resistance in the n layer. The top aluminum layer is 0.2 μm thick.

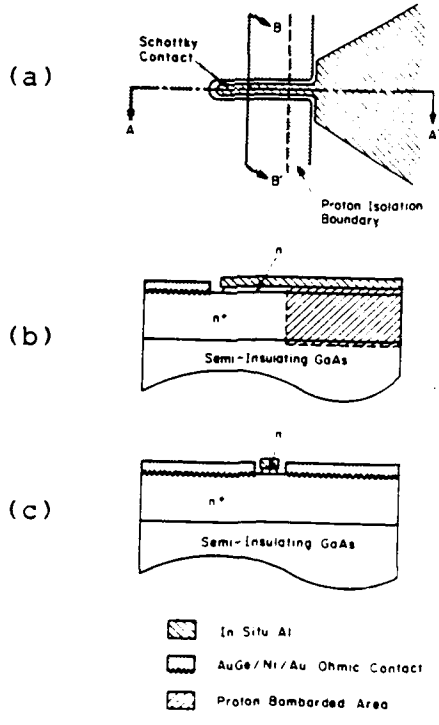

Fig. 3 Schottky diode structure (a), longitudinal section AA' (b) and cross section BB' (c).

The Schottky electrode is defined by a self-aligning process and proton isolation. The self-aligning process makes the Schottky electrode narrow and reduces the gap between it and the ohmic contact. The idea for this process comes from the closely spaced electrode (CSE) FET structure [4]. As shown in Fig. 4a, one photoresist mask first protects the Schottky electrode during etching and then defines the ohmic contact by lift off after evaporating AuGe/Ni/Au. With the proper undercut during etching, a 0.8 μm wide electrode (see Fig. 2d) has been achieved. After removing the photoresist, the ohmic contact is formed by alloying the evaporated AuGe/Ni/Au onto the n^+ layer at 430°C for 30 seconds in an H_2 ambient. The contact resistivity is determined to be 5 $\mu\Omega$-cm^2 by a transmission-line model [5].

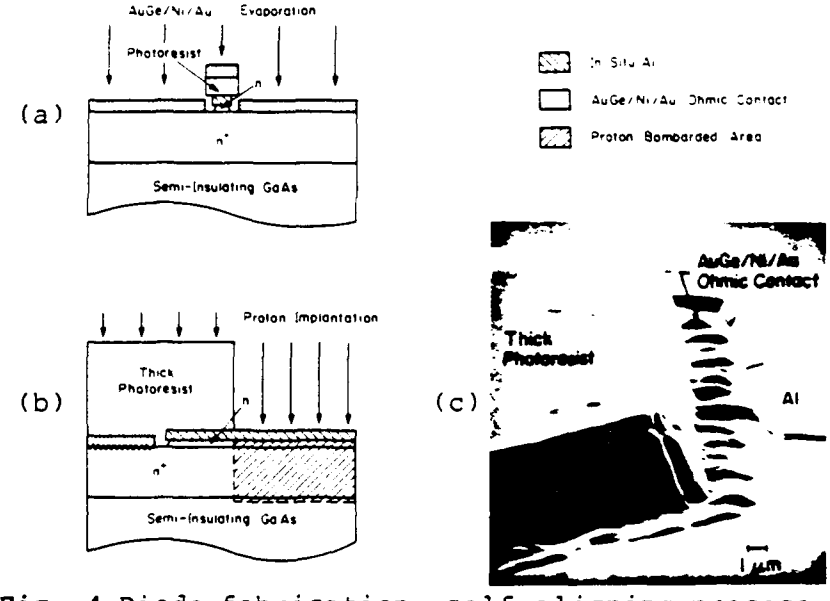

Fig. 4 Diode fabrication: self-aligning process (a), proton isolation (b), and the thick photoresist isolation mask (c).

The length of the diode is defined by proton bombardment (Fig. 4b). Proton isolation avoids the step coverage problem in mesa etching and is

easier than selective epitaxy [6,7]. Two consecutive proton implantations (320 keV with a $5x10^{14}$ cm^{-2} dose and 200 keV with a $3x10^{14}$ cm^{-2} dose) completely isolate our diodes [8]. Fig. 4c shows the photoresist mask. Note the sharp edge.

The series resistance, the ideality factor and the barrier height are obtained by a least-mean square fit of the diode equation to the measured current-voltage data [9]. After packaging, the measured series resistance is 15.9 Ω. This is in rough agreement with the value calculated from the diode geometry and the doping, 13 Ω [9]. The major part is contact resistance, 5.1 Ω. The ideality factor is 1.20, and the barrier height is 0.755 eV. The breakdown voltage (at 1 μA) is 5 V. The estimated zero-bias capacitance is 9 fF (5.5 fF junction and 3.5 fF parasitic). The cutoff frequency is 1.1 THz.

Fig. 5 shows the assembled array. The antenna leads are connected by 1-mil aluminum bond wires to 50-Ω striplines, which in turn are connected to SMA connectors. The silicon substrate lens is pressed against the chip by the nylon screws. The white polystyrene cap is put on the silicon lens to reduce the reflection loss [10].

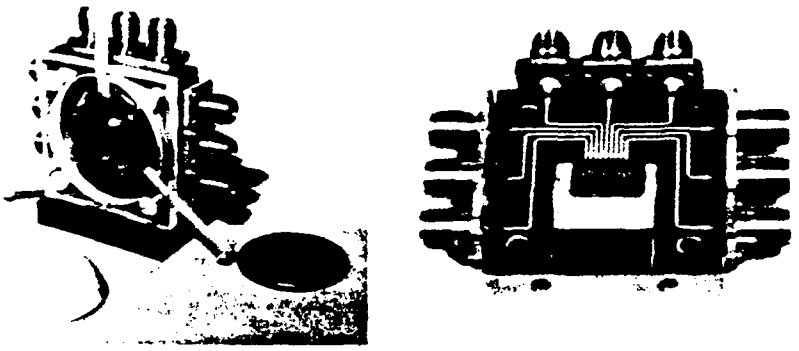

(a) (b)

Fig. 5 Assembled array from the front (a), with the plastic cap in the foreground, and from the back (b), showing the stripline IF connections and the array in the middle.

Video detection

Most of measurements were done at 94 GHz at Caltech. The signal is generated by a Gunn diode and square-wave modulated at 1 kHz. The signal radiates from a standard-gain horn. A TPX objective lens focuses the signal onto the array through a silicon substrate lens. Its focal length is calculated from the lens geometry to be 8.6 cm. The system video responsivity is calculated from the ratio of the diode output voltage to the signal power incident on the objective lens. The gain of the horn is calculated from its dimensions [11]. The 75-170 GHz measurements are done at UCLA with a similar set-up, except that the signal is generated by a backward-wave oscillator and modulated at 110 Hz.

System video responsivity versus bias current

Fig. 6 shows the theoretical 94-GHz system video responsivity versus bias current derived from the equivalent circuits of a Schottky diode video detector [9,12,13], which are fitted to the experimental data in dots by choosing a system coupling efficiency of 6.2 dB (24%). Table I gives the detailed loss breakdown. The losses due to lenses are estimated from data given by Afsar and Button [14].

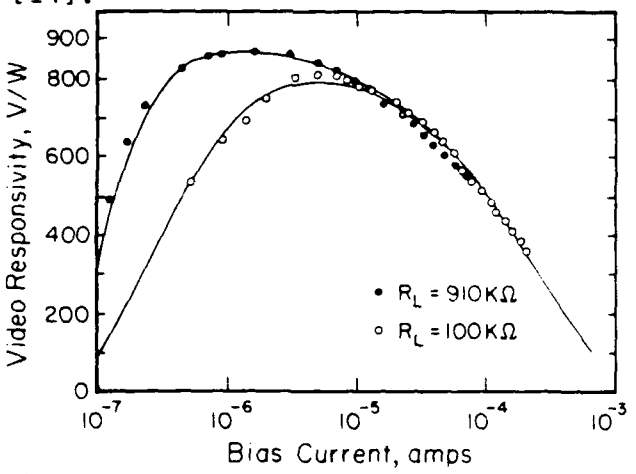

Fig. 6 The 94-GHz system video responsivity versus bias current at two different load impedances.

Table I Estimated system losses

TPX objective lens	0.3 dB reflection loss
	0.1 dB absorption loss
Polystyrene matching cap	0.1 dB reflection loss
Silicon lens	1.0 dB absorption loss
Antenna coupling efficiency	4.7 dB (34%)
System coupling efficiency	6.2 dB (24%)

System video responsivity versus frequency

In order to verify the circuit model, the system video responsivity was also measured from 75-170 GHz shown in Fig. 7. The solid line is calculated by the equivalent circuits of the a Schottky diode video detector [9,12]. It also includes the effect of the polystyrene cap [10]. Uncertainties in power-meter calibration factors and system losses contribute to the scatter in the experimental points. The 3dB cutoff frequency of the diode is about 140 GHz. One can see the circuit model works quite well over a frequency range of 75-170 GHz even though the skin effect is not taken into account. This is because all the metal and the epi-layer thickness is less than or equal to the skin depth. It also proves that the bow-tie antenna has an octave frequency bandwidth at least.

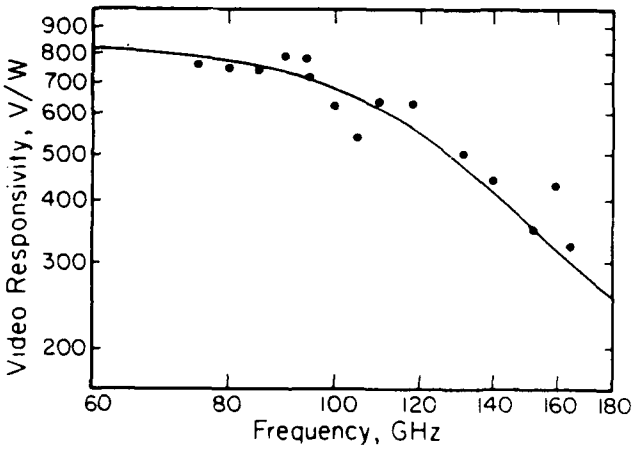

Fig. 7 System video responsivity versus frequency on a log scale.

System video responsivity versus aperture size

Fig. 8 shows the system video responsivity versus front aperture size. In this experiment, an aluminum plate with a hole in the middle serves as the aperture stop. For convenience, it is put on the backside of the objective lens. However, the input power is calculated from the front aperture size determined from the ray tracing diagram in Fig. 2b. By the same ray tracing diagram, the maximum angle α inside the silicon lens is found for each aperture size. This is also shown in Fig. 8. For aperture sizes larger than 3.6 cm, the maximum angle remains 59°, limited by the substrate lens. The diode is biased at 10 μA with a 100 KΩ load resistance. Fig. 8 shows a peak system video responsivity of 820 V/W at a 2.7 cm front aperture. This corresponds to a maximum angle of 45° (f/2.4 objective lens).

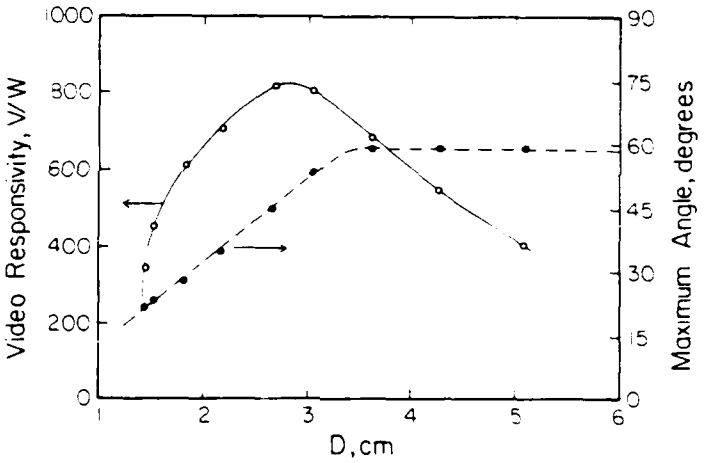

Fig. 8 System video responsivity and maximum angle inside the silicon lens versus front aperture.

This peak can be understood by considering spillover efficiency and taper efficiency [15]. The spillover efficiency causes the responsivity to decrease for small apertures because the Airy spot at the focal plane is larger than the effective area of the antenna. The power outside the antenna effective area will not be received efficiently. On the other hand, the responsivity

goes down for large apertures because the maximum angle is larger than the antenna beamwidth. The power outside the main beam will not be coupled efficiently into the detector.

Angular field of view of the imaging system

The imaging properties are obtained by studying both the angular field of view and the spot response. The angular field of view has been measured by rotating the entire receiver about the center of the objective lens as shown in Fig. 9 [16]. In this way it is possible to shift the focal spot from one antenna to the next. Fig. 10 shows the peak angle for each antenna and the system video responsivity for each antenna at its peak angle. The front aperture is 3 cm. The full field of view determined from the half power points is approximately 40°, with an angular separation between adjacent antennas of 7.4°. The off-center antennas roll off because rays miss the substrate lens (see Fig. 9). A larger substrate lens should reduce this loss.

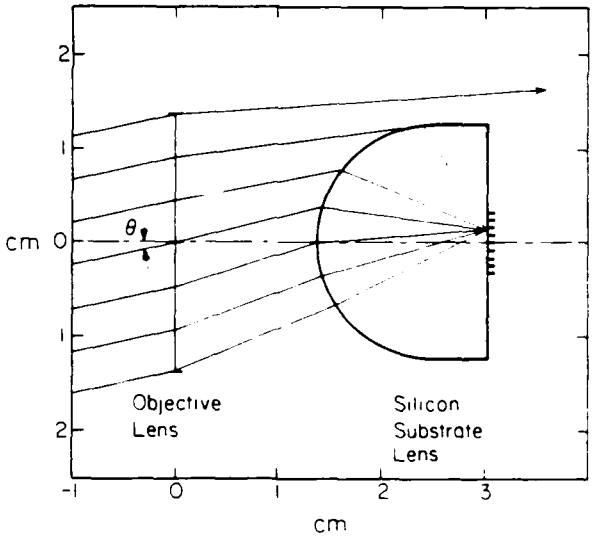

Fig. 9 The ray tracing diagram for a plane wave incident at an angle. Each tick at the interface represents an antenna. The ray on the top misses the silicon lens after focusing by the objective lens.

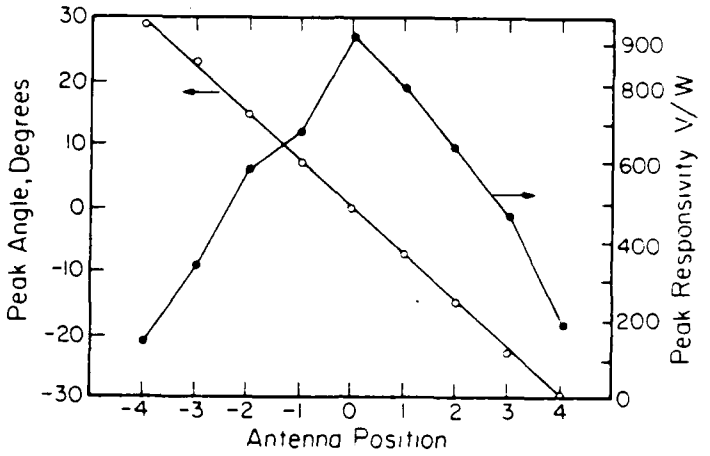

Fig. 10 Angular field of view of the 94-GHz imaging system with a 3-cm front aperture.

Spot response of the imaging system

Using the same rotation technique, we measure the spot response of the imaging system by monitoring the output of the center antenna while the incident angle changes. Fig. 11 shows the measured spot response in the H-plane, which corresponds to a rotation axis perpendicular to the imaging line. It also shows the theoretical Airy Pattern [17]. Although we use a 3-cm front aperture, the experiment data in circles fit the Airy pattern of a 2.5-cm aperture. Presumably this is due to non-uniform illumination of the aperture by the bow-tie antenna and edge effects of the aluminum stop. The triangles in Fig. 11 are the experimental data obtained by normalizing the output voltage from the adjacent antenna position to its peak system video responsivity shown in Fig. 10, when a plane wave is normally incident upon the objective lens. These also lie on the Airy pattern for a 2.5-cm aperture.

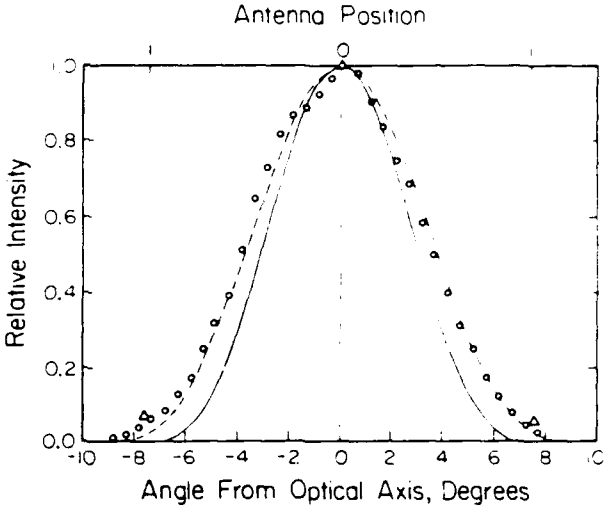

Fig. 11 Spot response for the 94-GHz imaging system with a 3-cm front aperture. Data in circles are obtained by the rotation technique. Data in triangles are obtained by the array with a plane wave normally incident upon the objective lens. The theoretical Airy patterns are shown with a solid line for a 3-cm aperture and a dash line for a 2.5-cm aperture.

Heterodyne detection

For double-side band heterodyne detection measurements, a dual-beam interferometer is used as a diplexer to combine the signal and the LO power into a single beam. It is designed to combine beams with negligible loss and suppress any LO noise within the sidebands [18]. The LO power at 91 GHz is generated by a klystron and can be adjusted by an attenuator. A low-noise IF amplifier chain with 80 dB gain and 106^{O}K noise temperature amplifies the IF power so that it can be measured by the HP435B power meter. It has a 1.4-GHz center frequency and a 200-MHz bandwidth. The mixer conversion loss and noise temperature are determined from hot and cold load measurements [19]. Microwave absorber (ECCOSORB CV3) at room temperature serves as the hot load.

The cold load is the same absorber, soaked in liquid nitrogen in a styrofoam box and reflected to the receiver by a metallic mirror. The absorber must cover the whole antenna beamwidth to get an accurate measurement. The mixer conversion loss and noise temperature include the loss and the noise from the mixer and the optical system but not from the IF amplifier chain.

Fig. 12 shows double-sideband mixer conversion loss and noise temperature versus LO power. Both conversion loss and noise temperature go down when the LO power increases. A DSB mixer conversion loss of 11.2 dB and noise temperature of 3370°K have been achieved with an LO power of 9 dBm. This conversion loss is divided into the following losses. The system coupling efficiency is 6.2 dB, inferred from video detection measurements. The intrinsic conversion loss is 0.9 dB for a broadband double-sideband mixer [20]. The RF and IF mismatch losses have been estimated from a computer program provided by Kerr and Siegel [21]. The calculated RF impedance is 80-j36 Ω, giving an RF mismatch loss of 0.2 dB and a series resistance loss of 1 dB. The calculated IF impedance is 150 Ω, giving an IF mismatch loss of 1.2 dB and series resistance loss of 0.5 dB. This leaves 1.2 dB unaccounted for. This is probably due to the bond wires and IF connections. Table II gives the complete conversion loss breakdown. We also made single-sideband measurements with a Gunn-diode sources as a check. The conversion-curves were similar in shape. The best SSB conversion loss was 14.4 dB, which is 3.2 dB worse than the DSB figure.

Table II The breakdown of DSB conversion loss

System coupling efficiency	6.2 dB
Intrinsic conversion loss	0.9 dB
RF mismatch	0.2 dB
IF mismatch	1.2 dB
RF series resistance loss	1.0 dB
IF series resistance loss	0.5 dB
Additional loss	1.2 db
DSB mixer conversion loss	11.2 dB

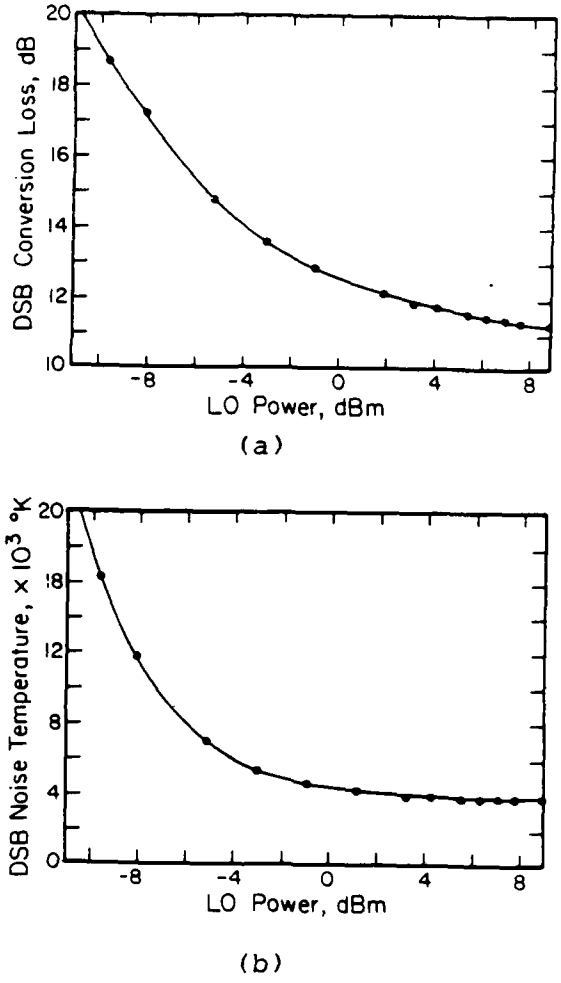

Fig. 12 Double-sideband mixer conversion loss (a) and noise temperature (b), versus local oscillator power.

The total receiver noise temperature including IF amplifier noise is 5170°K. As a passive total power radiometer, the minimum detectable temperature is 0.37°K with one second integration time and 200 MHz bandwidth.

Conclusion

This work has led to develop a compact millimeter-wave imaging array with high sensitivity. The measured diode conversion loss and system loss are both about 3 dB worse than the best room-temperature waveguide systems with whisker contacts [22]. The three obvious places for improvement are in the diode series resistance, the IF mismatch, and the antenna efficiency.

Acknowledgments

We appreciate the support of the Army Research Office and the Department of Energy. We are indebted to professors Amnon Yariv and Marc-Aurele Nicolet at Caltech for the use of their fabrication facilities, to Professor William Bridges at Caltech for loaning us millimeter-wave equipments, and to Professors Neville Luhmann and Harold Fetterman for the use of their facilities at the Center for Millimeter-Wave Electronics at UCLA. Thanks are also due to Mr. Frank So and Mr. Ali Ghaffari for proton implantation, to Mr. Perry McDonald for his assistance in the video measurements,and Mr. John Gilbert for taking SEM photographs.

References

[1] P. E. Young, D. P. Neikirk, P. P. Tong, D. B. Rutledge, and N. C. Luhmann, Jr., "Multichannel Far-infrared Phase Imaging for Fusion Plasmas," **Rev. Sci. Instrum. 56,** pp. 81-89, 1985.

[2] B. J. Clifton, G. D. Alley, R. A. Murphy, and I. H. Mroczkowski, "High-Performance Quasi-Optical GaAs Monolithic Mixer at 110 GHz," **IEEE Trans. Electron Devices, ED-28,** pp. 155-157, 1981.

[3] M. J. Wengler, D. P. Woody, R. E. Miller, and T. G. Phillips, "A Low Noise Receiver for Millimeter and Submillimeter Wavelength," to be published, **Int. J. of Infrared and Millimeter Waves.**

[4] T. Sugiura, H. Itoh, T. Tsuji, and K. Honjc, "12-GHz-Band Low-Noise GaAs Monolithic Amplifiers," **IEEE Trans. Microwave Theory Tech.,**

ED-30, pp. 1861-1866, 1983.
[5] H. H. Berger, "Models for Contacts to Planar Devices," **Solid-State Electronics, 15,** pp. 145-158, 1972.
[6] J. L. Heaton, W. Fabian, C. R. Snider, and F. H. Spooner,"Millimeter Wave GaAs Mixer Diodes Fabricated Using Selective Epitaxial Deposition or Deep Mesa Etching," **Proc. IEEE/Cornell Conf. on High-Speed Semiconductor Devices and Circuits,** pp. 47-59, Aug. 1984.
[7] J. A. Griffin, M. G. Spencer, G. L. Harris and J. Comas, "Formation of Planar n^+ Packets in GaAs for Mixer Diode Fabrication," **IEEE Trans. Electron Devices, ED-31,** pp. 1096-1099, 1984.
[8] J. P. Donnelly and F. J. Leonberger, "Multiple-Energy Proton Bombardment in n^+-GaAs," **Solid-State Electronics, 20,** pp. 183-189, 1977.
[9] C. Zah, "Millimeter-Wave Monolithic Schottky Diode Imaging Arrays," **Ph.D. Thesis,** California Institute of Technology, 1986.
[10] C. Zah and D. B. Rutledge, "A Polystyrene Cap for Matching Silicon Lens at Millimeter Wavelengths," to be published in **J. of Infrared and Millimeter Waves,** Sept. 1985.
[11] R. C. Johnson and H. Jasik, **Antenna Engineering Handbook,** Chap. 15, 2nd ed., McGraw-Hill, Inc., 1984.
[12] A. Kreisler, M. Pyee, and M. Redon, "Parameters Influencing for Infrared Video-detection with Submicron-Size Schottky Diodes," **Int. J. of Infrared and Millimeter Waves, 5,** pp. 559-584, 1984.
[13] Tai-Chi Wang "Components for Millimeter-Wave Integrated Circuits," **Ph.D. Thesis,** University of California, Berkeley, 1985.
[14] M. V. Afsar and K. J. Button, "Millimeter-Wave Dielectric Properties of Materials," **Infrared and Millimeter Waves,12,** Chap. 1, K. J. Button, ed., Academic Press, New York, 1984.
[15] C. Zah, R. C. Compton and D. B. Rutledge, "Efficiencies of Elementary Integrated-Circuit Feed Antenna," **Electromagnetics, 3,** pp. 239-254, 1984.
[16] D. P. Neikirk, "Integrated Detector Arrays for High Resolution Far-Infrared Imaging," **Ph.D. Thesis,** California Institute of Technology, 1984.
[17] M. Born and E. Wolf, **Principles of Optics,**

pp. 396, 6th ed., Pergamon Press, New York, 1980.
[18] P. F. Goldsmith, "Quasi-Optical Techniques at Millimeter and Submillimeter Wavelengths," **Infrared and Millimeter Waves, 6,** Chap. 5, K. J. Button, ed., Academic Press, New York, 1983.
[19] Bernd Vowinkd, "Simplified Receiver Response measurement," **Microwaves & RF**, pp. 147-148, 1984.
[20] A. J. Kelly, "Fundamental Limits on Conversion Loss of Double Sideband Resistive Mixers," **IEEE Trans. Microwave Theory Tech., MTT-25**, pp. 867-869, 1977.
[21] P. H. Siegel, A. R. Kerr and W. Hwang, "Topic in the Optimization of Millimeter-Wave Mixers," NASA Technical Paper 2287,Mar. 1984.
[22] J. W. Archer and M. T. Faber, "A very Low Noise Receiver for 80-120 GHz," **Int. J. Infrared and Millimeter Waves, 5,** PP. 1069-1081,1984.

International Journal of Infrared and Millimeter Waves, Vol. 7, No. 11, 1986

ADJUSTABLE TUNING FOR PLANAR MILLIMETER-WAVE CIRCUITS

Dylan F. Williams and S. E. Schwarz
University of California at Berkeley
Berkeley, California 94720

and
J. H. Sedlacek and D. J. Ehrlich
M. I. T. Lincoln Laboratory
244 Wood Street
Lexington, Massachusetts 02173

Received August 12, 1986

At millimeter wavelengths uncontrollable parasitics are often large enough to significantly degrade circuit performance when they are not compensated by adjustable elements. It is difficult to add adjustable elements to planar millimeter-wave circuits without increasing their size, weight, and cost. In this paper we investigate three adjustable elements, all involving movement of a short along a section of coplanar waveguide (CPW). These tuners are incorporated in a planar detector circuit for purposes of demonstration and characterization. Their losses are determined. The precision with which they can be adjusted is also considered. Of the three, a tuner based on the laser-assisted etching of molybdenum is shown to have the highest performance at millimeter wavelengths. This tuner employs laser direct write etching[1] with a recently developed photochemical reaction for trimming molybdenum.

Key words: Integrated circuit, laser etching, coplanar waveguide, adjustable backshort.

† University of California, Berkeley Berkeley, California 94720
* M.I.T. Lincoln Laboratory 244 Wood St. Lexington, Massachusetts 02173

0195-9271/86/1100-1729$05.00/0

Introduction

As frequency increases it becomes more difficult to obtain high performance from electronic circuits without the use of adjustable elements. This is a well known problem of planar millimeter-wave integrated-circuit technology, where uncontrollable parasitics are often large enough to significantly degrade circuit performance. It is possible to adjust a millimeter-wave integrated circuit by coupling it to a section of rectangular metal waveguide and then using standard methods of waveguide tuning to obtain an adjustable reactance, or by adjusting the distance between the planar circuit and a metal conductor suspended above it.[2,3] It is usually desirable to avoid such large mechanically adjustable elements, however, because of the added fabrication cost and the increase in size and weight of the integrated circuit.

In this paper we investigate three tuning methods suitable for use with millimeter-wave integrated circuits, all of which involve movement of a short along a section of coplanar waveguide (CPW). The electrical length of the CPW section is changed, and hence its reactance. This variable reactance may be used to cancel the effect of a parasitic reactance in the circuit by placing the two elements in series or in shunt with one another. Advantages of the integrated circuit are not lost when these tuning methods are employed, since the non-planar structures used to modify the length of the CPW are removed after the circuit is tuned. The losses and settability (the smallest increment with which the position of the short may be varied along the length of the CPW tuner) of these tuners are low enough to be suitable for use at millimeter wavelengths. A planar detector circuit has been used for demonstration at 33 GHz.

CPW Tuners

The first type of tuner, which we shall call the "strip tuner", makes use of a sequence of closely-spaced shorting strips, which can be removed one at a time to vary the position of the short. The strips are all fabricated simultaneously by the photolithographic process described in Table 1. The structure is shaped like a railroad track, the "ties" being the shorting strips. The "rails" play no role electrically, but serve to keep the shorting strips parallel and evenly spaced. The strips are thermo-compression bonded to the CPW. Since the "rails" and the thermo-compression bonds are both easily broken, the shorting strips can be removed one at a time mechanically without damaging the underlying conductors which compose the CPW. This changes the electrical length of the shorted CPW section. (One might think of using wire bonds for this purpose. However, the spacing between the conductors of CPW at millimeter wavelengths is very small. As a result, bonds made with a conventional bonding machine turn out to be much higher than they are wide, leading to problems of non-uniformity and excessive radiation. It is also difficult to obtain the small, uniform bond wire separations necessary at millimeter wavelengths.)

Step	Description
1.1	Clean wafers
1.2	Evaporate 450 Å of chrome and 2000 Å of gold
1.3	Apply and pattern AZ 4330 photoresist
1.4	Descum resist
1.5	Plate 20 μm of gold
1.6	Remove resist
1.7	Ion mill Gold and Chromium
1.8	Etch Chromium and lift off pattern

Table 1. The process steps used to fabricate the gold shorting strips.

The second tuner, called the "solder tuner", is illustrated in Fig. 2. Here the CPW section is coated with a layer of indium solder. A gold plate (also coated with a layer of indium solder) is held by a hot vacuum mount and lowered on a micrometer stage until it comes into contact with the layer of solder on the CPW section. The liquid solder then provides a good electrical contact between the conductors of the CPW section and the gold plate. The plate is free to slide over the CPW conductors which varies the position of the backshort. During the adjustment process the operation of the circuit can be continuously monitored. After the short has been adjusted to the desired position, the heat is turned off, the solder solidifies, and the cool vacuum mount is removed. Only the soldered gold plate is left on the circuit. It is found that the vacuum mount does not influence the circuit's operation significantly if precautions are taken to cool the semiconductor devices mounted on the circuit. Thus the circuit remains optimized when the soldering apparatus is removed.

The third tuner, called the "laser-etched tuner", is illustrated in Fig. 3. A layer of molybdenum is sputtered over the gold CPW conductors, shorting them together. The position of the short is changed by placing the circuit in a 200 torr flowing chlorine atmosphere and locally heating the molybdenum layer with a focused argon-ion laser beam. This stimulates the formation of volatile molybdenum chlorides which are carried away in the flowing chlorine atmosphere. The result is that the molybdenum is etched away, leaving the underlying gold CPW conductors intact. Scanning the beam across the guide successively exposes more of the CPW below the molybdenum layer, changing the effective position of the molybdenum short along the length of the CPW section. Etching is induced both pyrolytically and photochemically; at the incident power of ≈ 600 milliwatts employed in this experiment, both mechanisms are important.[4] For these

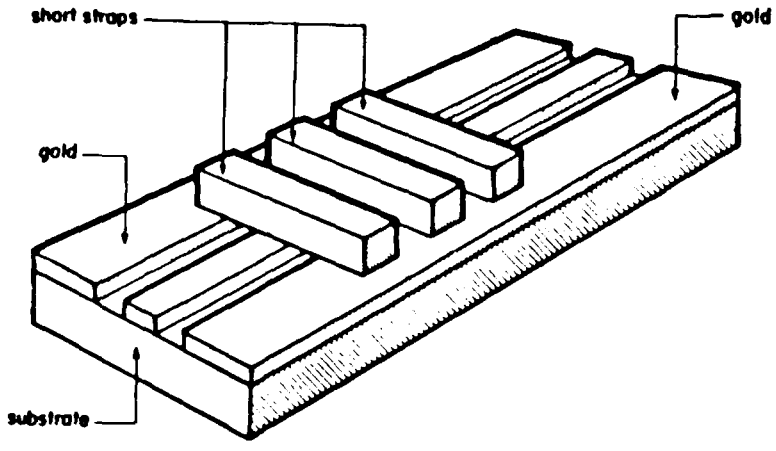

Fig. 1. Strip tuner in coplanar waveguide (CPW). The shorting strips are removed mechanically one at a time. This changes the effective position of the backshort, and hence, the admittance of the tuner.

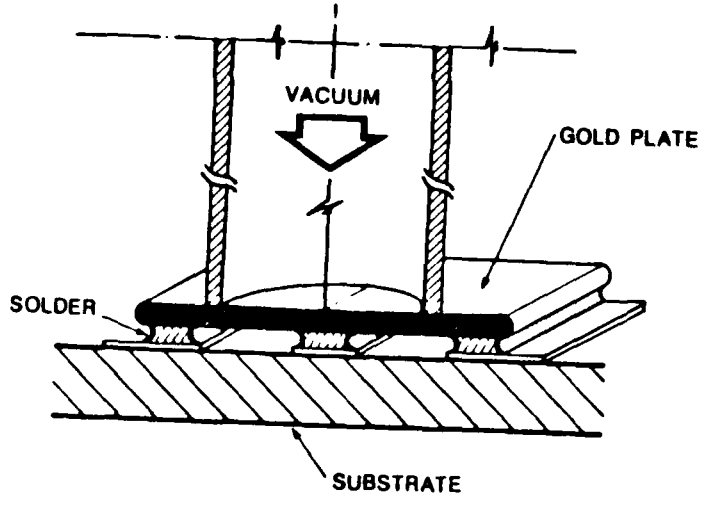

Fig. 2. Solder tuner in coplanar waveguide (CPW). The molten solder forms the electrical contact between the conductors of the CPW and the gold plate, shorting together the CPW conductors. The gold plate slides over the CPW conductors on the layer of molten solder. This changes the position of the short formed by the gold plate, and hence, the admittance of the tuner.

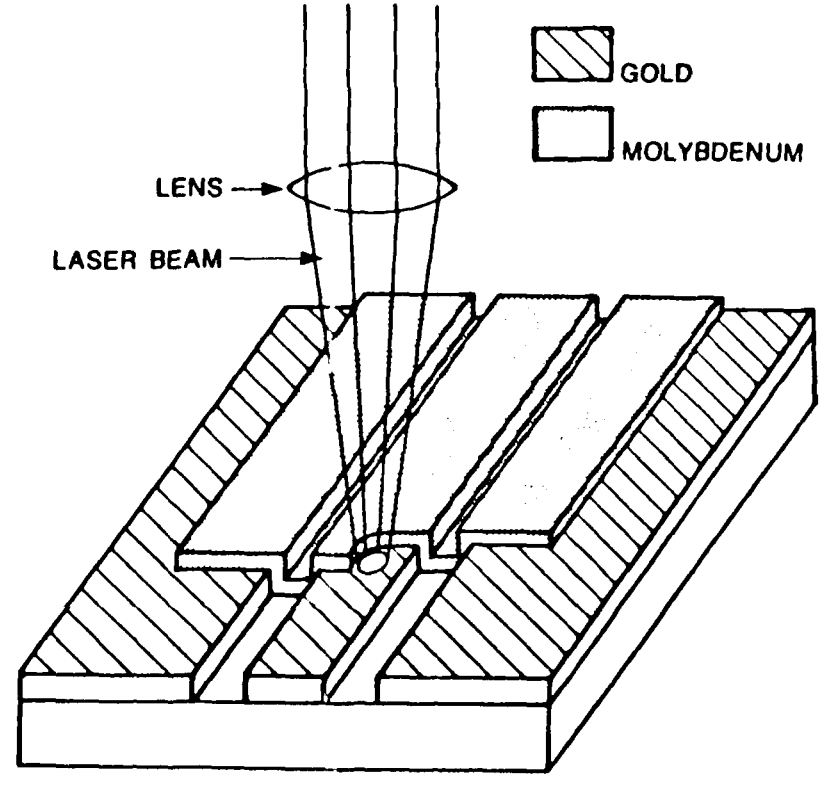

Fig. 3. Laser etched tuner in coplanar waveguide (CPW). The laser stimulates a local chemical reaction which etches away the molybdenum film shorting the gold CPW conductors. The effective position of the backshort is changed by moving the substrate forward slowly as the beam is scanned from side to side, progressively etching the molybdenum film away and exposing the gold CPW conductors underneath. This changes the position of the short formed by the remaining molybdenum, and hence, the admittance of the tuner. Submicron spatial resolution can be achieved permitting continuous tuning to with high precision. The laser etching is performed in situ as the device is exercised at millimeter-wave frequencies.

experiments, the laser beam was focused to a 2 μm spot size and scanned at a rate of 250 μm/sec. The distance between scans was set to 1 μm. The only undesirable effect of the laser etching process on the circuit was caused by heating of the circuit by the laser. The diode temperature was monitored by observing the bias conditions, which are temperature dependent. Since the circuit was suspended in the chlorine atmosphere at its edges, the rate of heat removal was very low, and the temperature of the circuit increased gradually during the etching process. This problem was circumvented by stopping the etching process after the diode temperature rose by about 15 C°. Provisions for efficient heat removal should be made in future work.

Tuner Characterization

An ideal tuner, when used to compensate for a shunt susceptance B, will have an admittance $Y_{tune} = -jB$, and the total admittance seen by the circuit will be zero. In practice, $Y_{tune} = -jB + j\,\Delta B_{tune} + G_{tune}$, where ΔB_{tune} is an error arising from inaccuracy in the backshort position and G_{tune} is a conductance due to losses. The total admittance seen by the circuit is thus $j\,\Delta B_{tune} + G_{tune}$. It is desirable to reduce both ΔB_{tune} and G_{tune}.

The loss of the transmission line used in the tuner is important because it determines the parasitic conductance G_{tune} of the tuner. The internal quality factor Q of a transmission line (as defined by Ramo, Whinnery, and Van Duzer[5]) is a measure of its loss and is defined as the ratio of the energy dissipated per cycle in the guide to the energy stored, for a section of line whose length is an integer multiple of a quarter of a guide wavelength. This Q is related to the complex propagation constant γ of the lossy transmission line by

$$\gamma = \alpha + i\beta' = i\beta\sqrt{1 - i/Q} \tag{1}$$

where α is the attenuation constant and β' is the propagation constant of the lossy transmission line and β is the propagation constant of the lossless transmission line. For the usual case where $Q \gg 1$, β and β' are approximately equal, and the Q may be related to the attenuation constant by

$$Q \cong \frac{\beta}{2\alpha} \tag{2}$$

The Q, as defined here, is dependent only on the intrinsic loss of the guide. The shunt conductance G_{tune} of the tuner is approximately given by[6]

$$\frac{G_{tune}}{Y_0} \approx \frac{1}{2Q}\left[\beta l\left(1 + \frac{B^2}{Y^2{}_0}\right) + \frac{B}{Y_0}\right] \tag{3}$$

where B is the susceptance to be tuned, $Q \gg 1$, Y_0 is the characteristic admittance of the transmission line of which the tuner is composed, and $B/Y_0 \lesssim 1$.

The settability Δl of the backshort is the smallest increment with which the position of the backshort may be adjusted. It is an important characteristic of the tuner because it determines the smallest achievable increment of tuner susceptance and, therefore, ΔB_{tune}. If $B/Y_0 \lesssim 1$, the quantity ΔB_{tune} is approximately given by[6]

$$\frac{|\Delta B_{tune}|}{Y_0} \approx \beta\Delta l\left(1 + \frac{B^2}{Y_0}\right) \tag{4}$$

If the losses of the tuner are small and resistive in nature, and the admittance Y_0 of the guiding medium, the propagation constant β of the guide when no losses are present, the settability Δl, and the internal quality factor Q of the guide are known, the admittance of the tuner Y_{tune} may be calculated exactly or approximated using equations (3) and (4). These parameters are sufficient for design calculations.

Under certain circumstances, the performance of the tuner can be easily estimated. If the tuner is placed in shunt with a load with conductance G_{load}, a source with conductance G_{source}, and a parasitic element with susceptance B, for instance, two ratios of interest are easily calculated. The first is P_{tuned}/P_0, where P_{tuned} is the power delivered to the load when the tuner is used and $G_{source} = G_{load}$ and P_0 is the power delivered to the load when the tuner is not used and G_{source} is chosen for maximum power transfer. P_{tuned}/P_0 represents the improvement in performance possible by incorporating the tuner in the circuit when the source conductance G_{source} may be chosen independently. A second ratio of interest is P_{tuned}/P_1, where P_1 is the power delivered to the load when $G_{source} = G_{load}$ and no tuner is used. P_{tuned}/P_1 represents the improvement in performance possible by incorporating the tuner in the circuit when the source conductance G_{source} is fixed. These ratios are given by

$$\frac{P_{tuned}}{P_0} = e_{tune}\,\frac{(1+\sqrt{1+(B/G_{load})^2})^2 + (B/G_{load})^2}{4\sqrt{1+(B/G_{load})^2}} \tag{5}$$

$$\frac{P_{tuned}}{P_1} = e_{tune}(1 + (B/2G_{load})^2) \tag{6}$$

where e_{tune}, the proportion of the available power delivered to the load when the tuner is in use, is given by

$$e_{tune} = \frac{1}{(1+G_{tune}/2G_{load})^2 + (\Delta B_{tune}/2G_{load})^2} \tag{7}$$

Detector Circuit

The three tuners described above were incorporated in the planar detector circuit shown in Fig. 4. Incident radiation is received by the slot

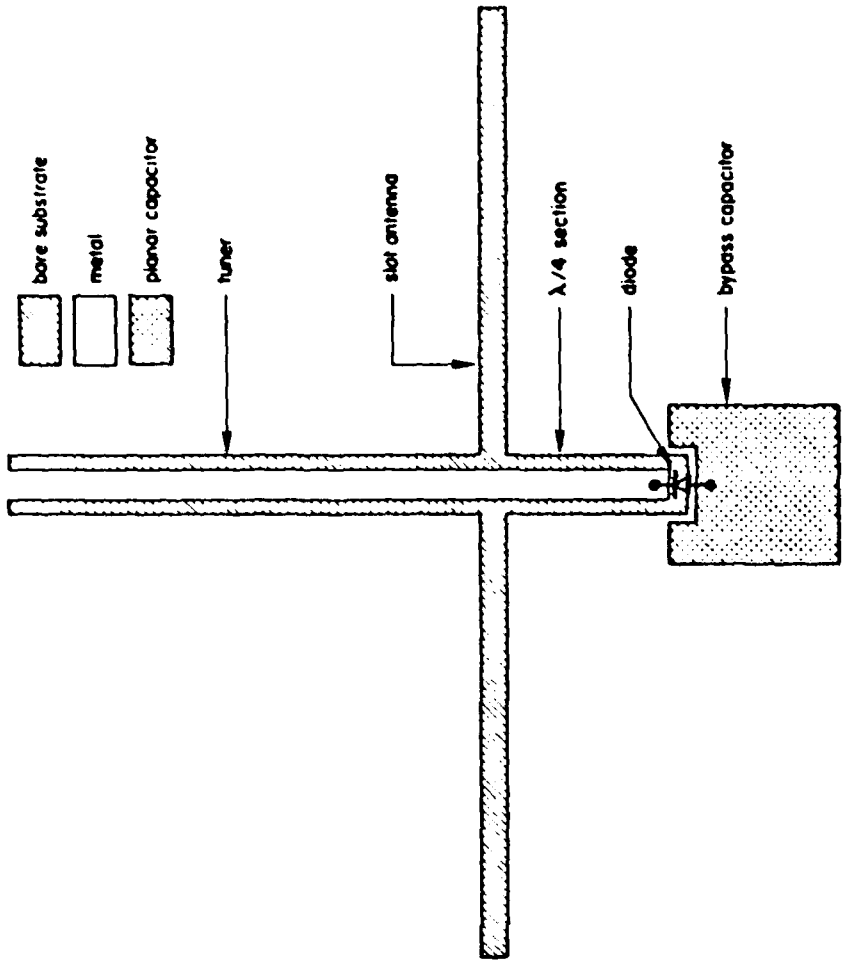

Fig. 4. Tunable detector circuit. The incident radiation creates a voltage across the slot antenna. The diode is placed at the end of the (approximately) quarter-wavelength CPW section. This transformer matches the slot impedance to the incremental resistance of the diode. The length of the tuner is adjusted to compensate for the parasitic diode capacitance.

antenna shown in the figure. A quarter-wavelength section matches the antenna impedance (about 3.3Ω) to the impedance of a silicon beam-lead diode biased to an incremental resistance of 418Ω. The CPW tuner is then used to compensate for the parasitic shunt capacitance of the diode. The CPW had a characteristic impedance of 50 Ω a total width of 296 μm, and a center conductor width of 148 μm. (The total width of the CPW was made about half the usual size to reduce radiation, which is difficult to model, although this results in additional ohmic loss.) The circuit was fabricated on a sapphire wafer. The fabrication process has been described earlier.[7]

The detected signal was measured as a function of the position of the backshort for the three tuners discussed above. Since the silicon diode has a rather high capacitance for use at 33 GHz, the improvement in performance over the untuned case ($l=0$ of Fig. 4) is quite significant. The model shown in Fig. 5 represents the detector circuit. The model parameters C_p, R_s, and C_j were obtained from the manufacturer of the diodes (Metelics Corp type MSS 40.141-B10, for which $C_j=0.20pF$ and $R_s=5\Omega$, were used for the strip and solder tuners and type MSS 40.140-B10, for which $C_j=0.05pF$, and $R_s=13\Omega$, for the laser-etched tuner). The value of C_p used in the model (.05 pF) was chosen to fit the observations. This value is larger than the .03 pF specified by the manufacturer; the difference probably arises from placing the diodes over the dielectric substrate. The incremental resistance of the diode is a function of both the bias conditions and the temperature, and was 418 Ω for the strip tuner, 428 Ω for the laser-etched tuner, and 525.6 Ω for the solder tuner (which was operated at a significantly higher temperature). All of the other parameters of the model (except the Q of the CPW lines and the value of L_p) were derived from low frequency measurements of scale models. The value of L_{ser} was determined from scale model measurements to be 0.020 nh for the laser-etched tuner and 0.015 nh for the strip and solder tuners; the difference being due to the different thicknesses of the 5000Å molybdenum film and the 20 μm shorting straps and gold plates.

The Q of the transmission lines in the actual circuit were estimated by fitting the tuning curves generated from the equivalent circuit to the measured tuning curves shown in Figs. 6-8. The Q and the value of L_p were considered to be adjustable parameters of the model. The value of L_p was considered to be adjustable because it depends both on the method of installation and on the diode type. The shape of the curve was quite sensitive to L_p; this allowed us to estimate the value of L_p. The values of L_p which gave the best fit to the experimental data shown in Fig. 6-8 were .11 nh, .11 nh, and .04 nh respectively. Then the Q was determined by comparing the measured and calculated ratios of $V_{det}(\beta l_{max})/V_{det}(\beta l=0)$, where $V_{det}(\beta l)$ is the voltage response of the diode when the length of the tuner is l. $V_{det}(\beta l_{max})$ was the voltage response when the device was tuned for maximum responsivity and $V_{det}(\beta l=0)$ is the voltage response of the

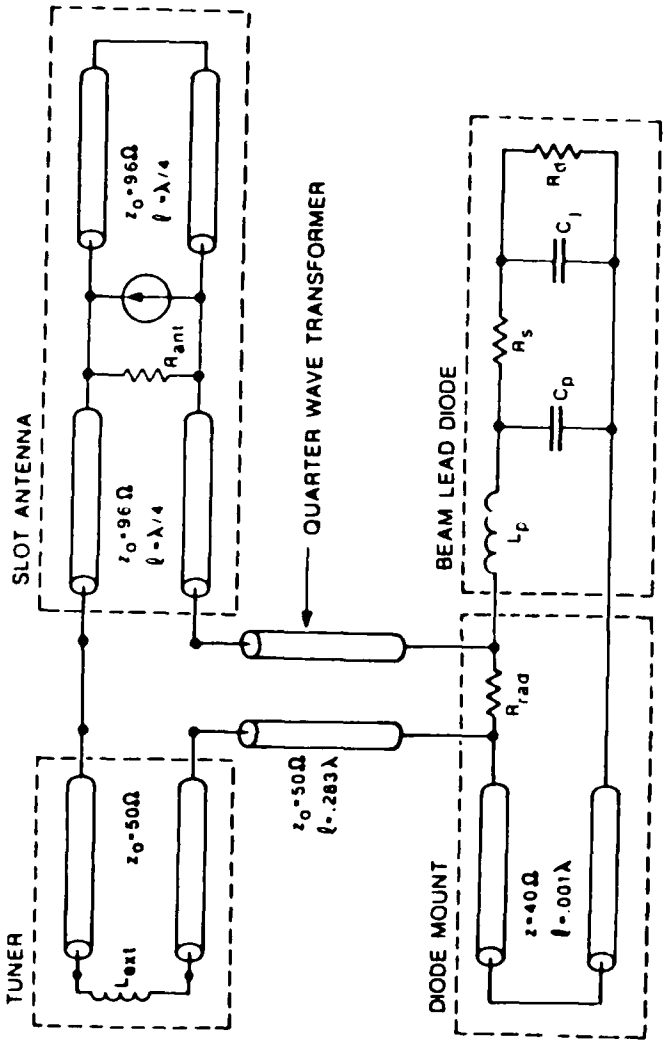

Fig. 5. The model used to analyze the detector of Fig. 4. The circuit values are $R_{ant}=696\,\Omega$, $R_d=417\,\Omega$, $R_{rad}=4000\,\Omega$. The other circuit values are given in the text.

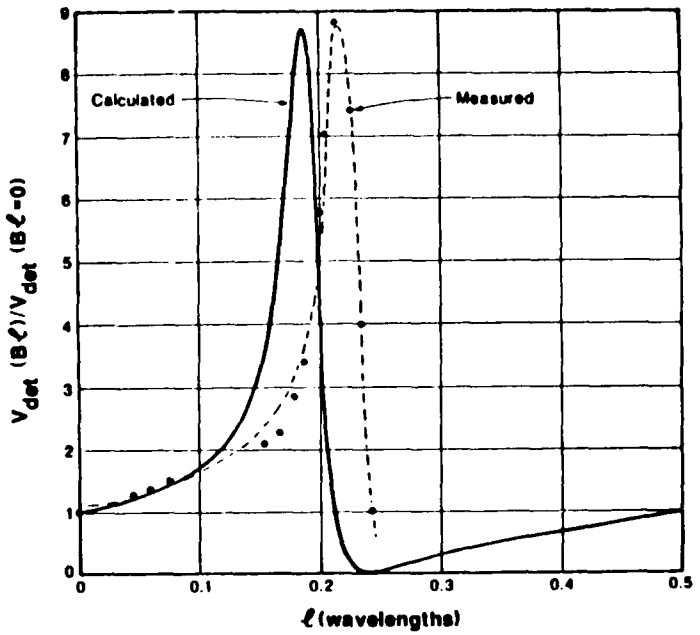

Fig. 6. The measured and calculated responses of the detector utilizing the strip tuner as a function of backshort position.

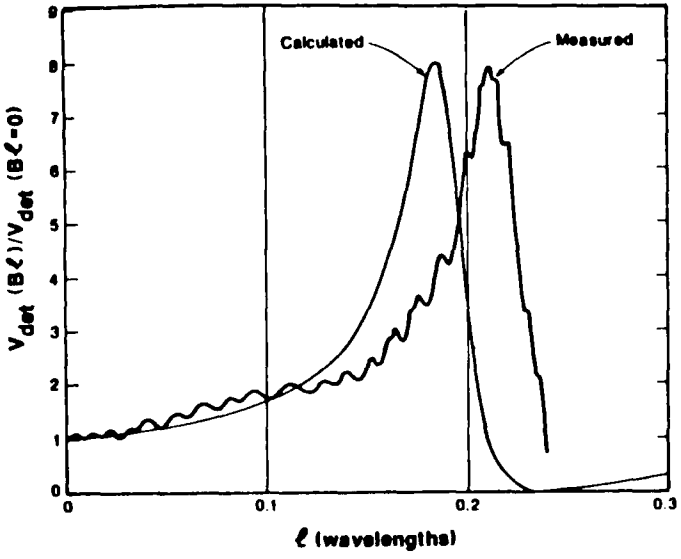

Fig. 7. The measured and calculated responses of the detector utilizing the solder tuner as a function of backshort position.

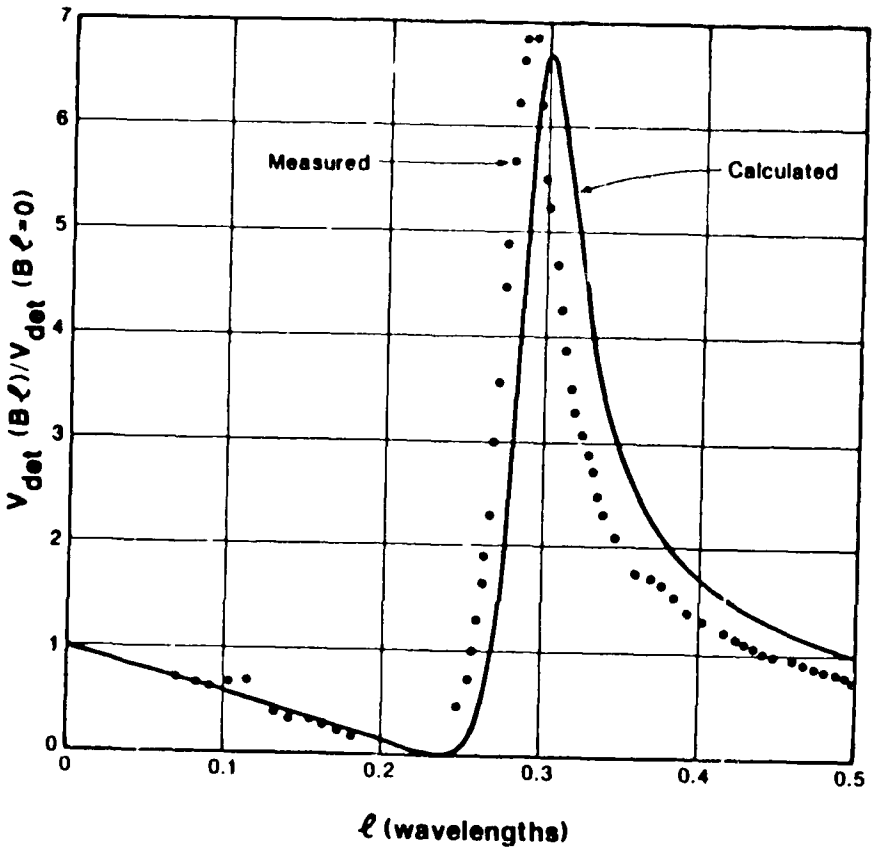

Fig. 8. The measured and calculated responses of the detector utilizing the laser-etched tuner as a function of backshort position.

diode when the length of the tuner was zero. The resulting value of Q contains a small uncertainty because the ratio $V_{det}(\beta l_{max})/V_{det}(\beta l=0)$ also depends weakly on the value of L_p.

For the strip tuner, the Q's of all of the transmission lines in the equivalent circuit were assumed to be the same. (This assumption is justified because the transmission line used for the tuner is identical to the transmission line used for the quarter wave transformer.) Agreement of the measured and calculated values of the ratio $V_{det}(\beta l_{max})/V_{det}(\beta l=0)$ was found to occur for Q's between 100 and 150. This is to be compared with a predicted Q of 130 for these lines[8] (using values of 0.0535 Ω/□ and 1×10^{-4}, for the surface resistance of the gold film and loss tangent of the sapphire substrate, respectively). It is not surprising that the measured and calculated backshort positions which gave the maximum response were different since it was difficult to accurately determine the number of strips which had been removed.

The Q's of the solder tuner and the laser tuner were found by assuming that the Q's of all the transmission lines in the equivalent circuit except the tuners themselves were equal to 130. Again, calculated and measured values of the ratio $V_{det}(\beta l_{max})/V_{det}(\beta l=0)$ were compared. The Q of the solder tuner was estimated to be about 50 by this method. The lower Q of the solder tuner is believed to be due to the presence of flux. (An attempt was made to tune the detector circuit in a nitrogen atmosphere without using flux, but the solder did not form a good contact between the waveguide and the suspended gold plate.) Again, the position of the backshort could not be determined accurately for the solder tuner, and the calculated and measured curves do not show the same position of the maxima.

Molybdenum Backshort

The Q of the laser-etched tuner was estimated by the above procedure to be about 130. Within the accuracy of the technique, this is the same as that estimated for the strip tuner. In this case, the device was mounted on a computer controlled stage, and the position of the backshort could be determined very accurately. The measured and calculated curves are in very close agreement.

The molybdenum film used in the laser-etched tuner backshort has a resistivity of about four times that of gold and was less than half as thick as the layer forming the gold CPW conductors. It seems curious that the Q of the of the laser-etched tuner should be about the same as that of the strip tuner, since the 5000Å thick molybdenum backshort might be expected to be quite resistive.

To solve for the impedance Z of a molybdenum backshort a complicated boundary value problem must be solved.[9] It is possible, however, to estimate the impedance of the backshort easily in the two limits of either

very high or very low loss. In the limit of very high loss, the backshort may be modeled as a CPW transmission line shunted by the lossy molybdenum layer. In this limit the impedance Z of the backshort has equal real and imaginary parts. As the surface resistance of the molybdenum film becomes smaller, this model predicts that the impedance of the backshort approaches zero.

In the limit of very low loss, the impedance of the backshort becomes purely inductive because the short has some external inductance. In this case, the impedance of a planar CPW backshort becomes $Z \cong j\omega L_{ext}$, where L_{ext} is the external inductance of the backshort. This is not consistent with the transmission line model of the lossy backshort, which fails for highly conductive films, and predicts that Z has equal real and imaginary parts and that the absolute value of Z approaches zero as the resistivity of the molybdenum approaches zero.

In general, both limits must be considered, since both the resistive loss of the molybdenum and the external inductance contribute to current penetration into the backshort. The farther the currents penetrate into the conductor, the lower the resistance of the backshort. Since both effects increase current penetration, the actual resistance of the backshort is lower than that predicted by either model, and the models can be considered to give upper bounds on the resistance of the backshort. After exploring these two limits, we will show that for our case the estimated backshort resistance is consistent with the low measured loss of the laser-etched tuner.

Under the assumption of high loss, the resistance of the molybdenum backshort is estimated by modeling it as a lossy transmission line with a shunt conductance per unit length G given by

$$G = \frac{2t}{\rho_{moly} w} \tag{8}$$

where t is the thickness of the film, w is the width of the slots in the CPW, and $\rho_{moly} = 5.78 \times 10^{-6}\,\Omega$ cm is the resistivity of molybdenum. (The factor of two in equation (8) is a result of there being two slots shorted by the molybdenum in shunt across the transmission line. The skin depth does not enter since in this case it is greater than t, the thickness of the molybdenum. If the skin depth of the molybdenum were less than t, G would become complex.) The characteristic impedance Z of the backshort is then given by[5]

$$Z = \sqrt{j\omega L / (G + j\omega C)} \tag{9}$$

and the propagation constant γ by

$$\gamma = \sqrt{j\omega L (G + j\omega C)} \tag{10}$$

where L is the inductance of the line per unit length, C is the capacitance of the line per unit length, and ω is the angular frequency. (The values of L and C are most easily found by looking up the quasi-static values for Z and γ in tables[10] and solving for L and C under the assumption that G is zero. Then the actual values of Z and γ are found from L, C, and G.) For our backshorts (with $t = 5000$ Å, $w = 75\,\mu$m, $\epsilon_r = 10.5$, and a quasi-static impedance of $50\,\Omega$), $Z = (1 + j)0.4\,\Omega$ and the wave decays to its $1/e$ point in a distance $d_{lossy} = 11\,\mu$m. This $0.4\,\Omega$ resistance is large enough to have reduced the measured Q to approximately 50.

Rosa gives a formula for the external inductance of a thin perfectly conducting strip[11,12]

$$L_{ext} \approx 2 w_{ind} (\ln(2\pi w_{ind} / d_{ind}) - 1 + d_{ind} / w_{ind}\pi)\ nh \tag{11}$$

where d_{ind} is the width of the strip and w_{ind} is the length of the strip in cm. Under the assumption of low loss, the molybdenum backshort may be modeled as two strips of length w_{ind} approximately equal to the width of the slots between the CPW conductors and width d_{ind}, where d_{ind} must still be determined. Physically, the quantity d_{ind} corresponds approximately to the depth of current penetration into the backshort. The external inductance L_{ext} of a low loss backshort may be measured at low frequency. The quantity d_{ind} may be estimated by setting the inductance calculated from equation (11) equal to the external inductance measured at low frequency. The resistance of the backshort may be estimated from d_{ind}, the approximate depth to which the currents penetrate into the molybdenum conductor, to be $Z \approx w \rho_{moly} / (2 d_{ind} t)$. For our backshort, for which $L_{ext} \approx 0.02$ nh and $w_{ind} \approx 90\,\mu$m (w_{ind} is chosen to be slightly larger than w, the width of the slots, since the currents must travel around the ends of the short), $d_{ind} \approx 25\,\mu$m, which is considerably larger than d_{lossy}. From this we conclude that the currents penetrate much farther into the backshort than would be expected in the lossy model. This implies the surprising (and fortuitous) result that, because of the current spreading due to the external inductance of the backshort, the resistance of the backshort is on the order of only one tenth of an ohm, which is small compared to the ohmic conductor loss of the CPW section.

Conclusion

The Q due to ohmic loss is proportional to the width of the CPW, which was only half of the usual width, so the Q of these tuners could easily be doubled by doubling the width of the guide. Since the Q of the guide is dominated by ohmic loss, the expected Q as a function of frequency of these wider lines (based on skin depth formulas[5]), is

$$Q \approx 1494 / \sqrt{f} \tag{12}$$

for the strip and laser-etched tuners and

$$Q \approx 689 / \sqrt{f} \tag{13}$$

for the solder tuner where f is the frequency in GHz and the dielectric constant of the substrate is equal to 10.5. The settability of the strip and

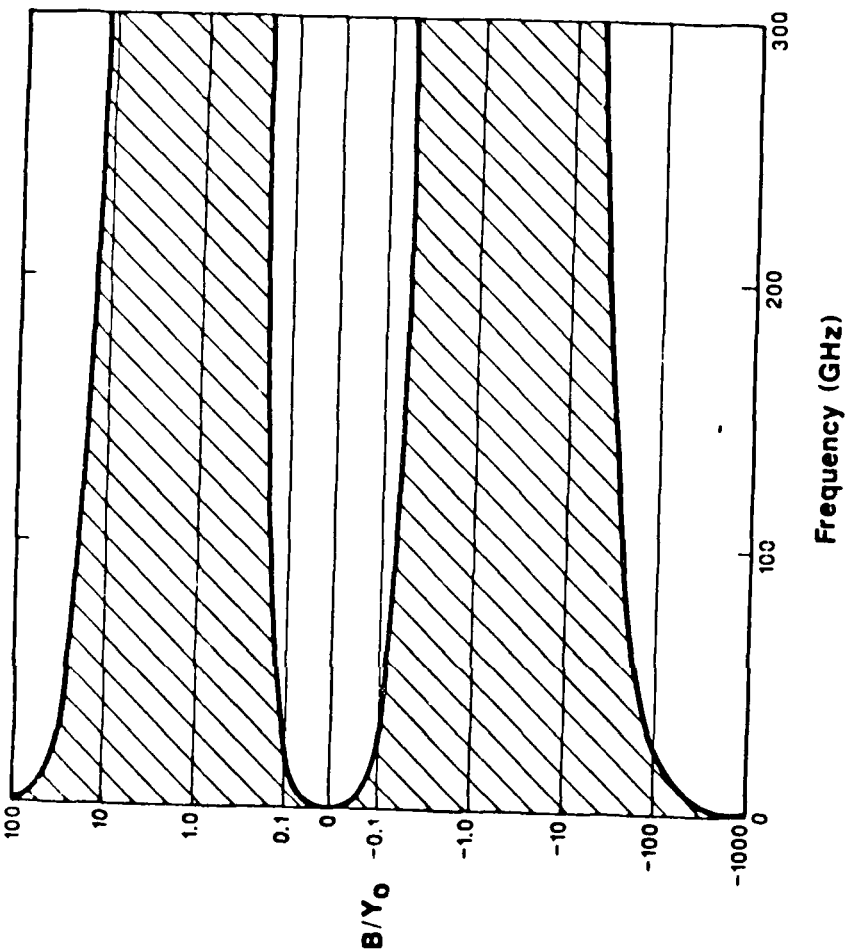

Fig. 9. The region for which P_{tuned} / P_0 is greater than one is shaded for the laser-etched tuner. This region represents the region for which incorporating the tuner gives an improvement in circuit performance under the assumptions stated in the article and the source conductance may be chosen independently. The Q of the tuner is assumed to be given by equation (12) and the settability of the tuner is assumed to be 1 μm.

solder tuners was about 32 μm. This value could easily be reduced by a factor of 3 if improvements in the positioning apparatus were made. The settability of the laser-etched tuner was 1 μm, but settabilities of 0.5 μm or less are possible.[4] Since the laser-etched tuner has losses limited by the guiding medium itself and settability an order of magnitude lower than the strip and solder tuners, it is the tuner most suitable for use at millimeter wavelengths. In Fig. 9 the ranges of B / Y_0 for which $P_{tuned} / P_0 > 1$ (see equation (5)) are shown as a function of frequency where the Q of the tuner is given by equation (12) and the settability of the tuner is assumed to be 1 μm. This region represents the region in which the laser-etched tuner is expected to be useful.

Additional improvements in these tuners can be realized by making the substrate thinner or by reducing its dielectric constant. If the dielectric constant is reduced to 2.5, for example, the Q would be increased by a factor of about 3.4, assuming that dielectric loss may be neglected. The value of β would be reduced by a factor of about 1.8, which allows the tuner reactance to be varied in smaller increments.

Acknowledgement

The authors would like to thank Ken Kundert for providing and modifying the circuit simulation tools used in this work. This research was supported in part by the National Science Foundation under grant ECS-85-00992 and by a U. S. Army Research Office fellowship under grant DAAG 29-83-G-0014. The Lincoln Laboratory portion of this work was sponsored by the Department of the Air Force, in part under a specific program supported by the Air Force Office of Scientific Research, by the Defense Advanced Research Projects Agency, and by the Army Research Office.

References

1. D. J. Ehrlich and J. Y. Tsao, "A review of laser-microchemical processing," *Journal of Vacuum Science Techonlogy*, vol. B1, no. 4, pp. 969-984, October-December 1983.
2. T. F. Finnegan and O. H. Soerensen, "Adjustable microstrip transformer for use with josephson devices in mm-wave ICs," *Electronics Letters*, vol. 17, no. 2, pp. 79-80, 22 January 1981.
3. D. F. Williams and S. E. Schwarz, "Design and performance of coplanar waveguide bandpass filters," *IEEE Trans. Microwave Theory and Tech.*, vol. MTT-31, no. 7, pp. 558-566, July 1983.
4. H. Rothschild, J. H. C. Sedlacek, and D. J. Ehrlich, "Photochemical laser etching of Mo and W thin films," *to be published*.
5. S. Ramo, J. R. Whinnery, and T. Van Duzer, *Fields And Waves In Communication Electronics*, John Wiley and Sons, New York, 1984.

6. D. F. Williams, "Millimeter-Wave Integrated Circuit Technology," *Phd. Thesis*, University of California, Berkeley, July 1986.

7. D. F. Williams and S. E. Schwarz, "A planar subharmonically-pumped 71 GHz receiver with integral feed antenna," *International Journal of Infrared and Millimeter Waves*, vol. 7, no. 2, February 1986.

8. D. F. Williams and S. E. Schwarz, "Reduction of propagation losses in coplanar waveguide," *Proceedings of the 1984 IEEE International Microwave Symposium*, pp. 453-454, July 1984.

9. K. C. Gupta, R. Garg, and I. J. Bahl, *Microstrip Lines and Slotlines*, Artech House, Dedham, MA, 1979.

10. M. E. Davis, E. W. Williams, and A. C. Celestini, "Finite-boundary corrections to the coplanar waveguide analysis," *IEEE Trans. Microwave Theory and Tech.*, vol. MTT-21, pp. 594-596, September 1973.

11. E. B. Rosa and F. W. Grover, "Formulas and tables for the calculation of mutual and self-inductance," *Uninted States National Bureau of Standards Bulletin*, vol. 8, no. 1, pp. 1-237, January 1912.

12. E. B. Rosa, "The self and mutual inductances of linear conductors," *Uninted States National Bureau of Standards Bulletin*, vol. 4, no. 2, pp. 301-344, January 1907.

International Journal of Infrared and Millimeter Waves, Vol. 7, No. 11, 1986

THEORY OF THE TRANSMISSION OF METAL STRIP GRATINGS ON A DIELECTRIC SUBSTRATE APPLICATION TO SUBMILLIMETER LASER COUPLING

J. P. Creen and D. Vèron

Association EUR-CEA sur la Fusion Contrôlée B.P. no. 6
F-92265 Fontenay-aux-Roses, France

and

P. Belland

Laboratoire de Dispositifs Infrarouge
Université Paris VI
4 place Jussieu
F-75252 Paris Cedex 05, France

Received July 20, 1986

The advantages of supported metal strip gratings with respect to free-standing metal meshes are pointed out for applications as laser output couplers. A new, simple formula for the power transmission through the strip grating on a dielectric plate is derived from a line equivalent-circuit model. This formula is in good agreement with measurements performed on several samples, at different submillimeter wavelengths. An application to output couplers of far-infrared gas discharge lasers allows to improve the reliability of such lasers.

Key words: dielectrically backed metal strip gratings, submillimeter laser output couplers.

* Unité associée au CNRS.U.A 836.

0195 9271/86/1100-1747$05.00/0

High-Accuracy Tuning of Planar Millimeter-Wave Circuits by Laser Photochemical Etching

D. J. EHRLICH, D. F. WILLIAMS, J. H. C. SEDLACEK, M. ROTHSCHILD, AND STEVEN E. SCHWARZ, SENIOR MEMBER, IEEE

Abstract—A new laser photochemical reaction for etching of molybdenum has been applied to the *in situ* tuning of coplanar waveguide (CPW) structures used in millimeter wave integrated circuits. Tests on structures operating at 33 GHz have confirmed low insertion losses and demonstrated an improvement in set accuracy by a factor of 10-30 relative to previously developed strip or solder tuners.

LASER direct-writing techniques based on rapidly scanned microscopic etching and deposition reactions have been recently developed [1]. By avoiding multistep lithography and conventional pattern transfer, these techniques provide important leverage via final-step microfabrication operations such as logic personalization, fault avoidance, and defect repair on integrated circuits. In addition, this technology presents new capabilities for trimming and tuning of analog devices. For these applications, advantages of direct-write etching over previous physical-probe and laser ablation methods are low induced temperature, greater spatial resolution, and elimination of debris and nonselective substrate damage.

Here we describe the use of a recently developed laser direct-write etching reaction [2], [3] to achieve high-accuracy tuning of planar millimeter-wave circuits. With the recent improvements of these circuits, adjustable elements are becoming important as a means to control limiting parasitics. We find that, in comparison to other methods currently under development, laser etching permits tuner settabilities of one-to-two decades greater accuracy. The new method could be useful as an automated post-fabrication trimming operation to produce highly precise matched devices.

Laser direct-write tuning was demonstrated with the planar circuit shown in Fig. 1. Incident radiation is received by the slot antenna. A quarter-wavelength section matches the antenna impedance (3.3 Ω) to the impedance of a silicon beam-lead diode biased to an incremental resistance of 428 Ω. The coplanar waveguide (CPW) tuner is then used to compensate for the parasitic shunt capacitance of the diode (Metallics Corp., type MSS 40, 140-B10). The CPW had a characteristic impedance of 50 Ω, a total width of 296 μm, and a center conductor width of 148 μm. The circuit fabrication process is described in [4]. Laser tuning is accomplished by stepwise etching of a 500-nm-thick molybdenum shorting film sputtered over the CPW. Scanning of the focused laser beam across the guide successively exposes more of the CPW below the Mo layer, changing the effective position of the Mo backshort along the length of the CPW section. The etching process exhibits high material selectivity, leaving the underlying 1-μm-thick gold film and sapphire substrate intact.

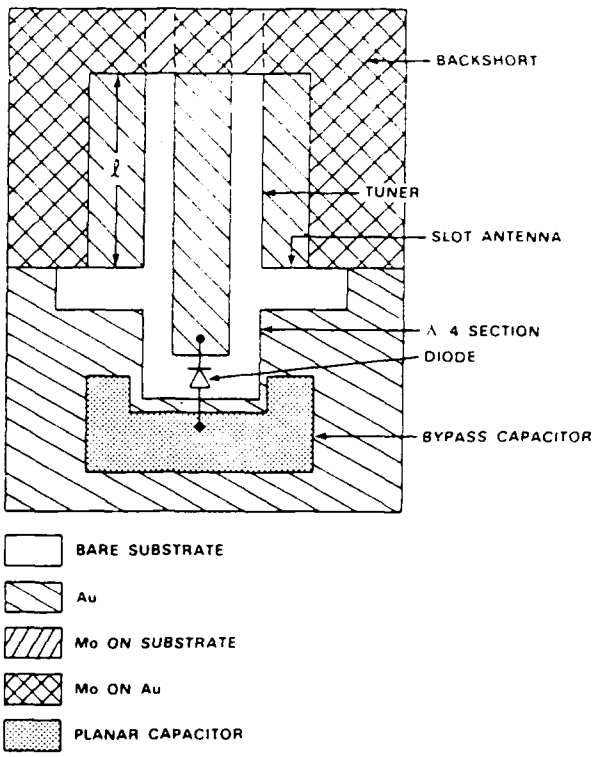

Fig. 1. Tunable detector circuit. The incident radiation creates a voltage across the slot antenna. The (approximately) λ/4 section matches the slot impedance to the incremental resistance of the diode. The length of the tuner l is adjusted to compensate for the parasitic diode capacitance by stepwise photochemical etching of the molybdenum backshort.

The laser direct-writing instrument was similar to those described previously [1]. A 600-mW 488-nm wavelength

Manuscript received November 5, 1986; revised December 23, 1986. This work was supported by the Defense Advanced Research Projects Agency, the Army Research Office, and the Department of the Air Force, under a specific program sponsored by the Air Force Office of Scientific Research. Research at Berkeley was supported in part by the National Science Foundation under Grant ECS-85-00992 and by a U.S. Army Research Office Fellowship under Grant DAAG 29-83-G0014.

D. J. Ehrlich, J. H. C. Sedlacek, and M. Rothschild are with M.I.T. Lincoln Laboratory, Lexington, MA 02173.

D. F. Williams was with the Department of Electrical Engineering, University of California, Berkeley, CA 94720. He is now with Ball Aerospace, Boulder, CO 80306.

S. E. Schwarz is with the Department of Electrical Engineering, University of California, Berkeley, CA 94720.

IEEE Log Number 8613460.

0741-3106/87/0300-0110$01.00

beam was scanned across the tuner in the presence of a 200-torr flowing Cl_2 ambient. Scanning was performed with a computer-controlled translation stage at a speed of 250 μm/s. In this first demonstration, the laser beam was focused to a 2-μm spot, and the scan separations were set at 1 μm. With optimized performance these values can be reduced to <1 μm and <0.25 μm, respectively.

The laser etching of molybdenum thin films with a Cl_2 ambient is a highly precise photochemical reaction which has been developed recently [2], [3]. The mechanism comprises two components. In one, the argon-ion laser photolyzes both the vapor ambient and a Cl_2 adsorbed surface layer. This generates reactive Cl atoms and bypasses the high-temperature thermal dissociation of Cl_2 which would otherwise be required. In the second component, the laser generates moderate localized heating of the molybdenum film, accelerating surface reactions which evolve volatile molybdenum chlorides. The ratio of these two components is continuously adjustable by variation of the incident laser power, and is chosen to maintain an optimal trade-off in temperature versus resolution and etching rate. We note that several other halide-based laser etching reactions in which there is no photochemical component are not acceptable for the current application [3]. In the demonstration here the tuning rate was limited by the software in the control computer, rather than the reaction rate (or stage speed), and a relatively low-power level, favoring low temperature, was chosen. More detail about the relevant chemical kinetics can be found in [2] and [3].

In the present demonstration the circuit was operated at 33 GHz and the diode voltage response V was monitored *in situ* during laser etching of the Mo backshort. Fig. 2 represents the experimentally measured variation of V with tuner length l. $V(l)$ is normalized to the diode response for the untuned device $V(l = 0)$. A more than six-fold improvement is noted at $l = 0.28$ λ (λ is the guide wavelength at 33 GHz).

An equivalent-circuit model was used to analyze the circuit in Fig. 1. Two variable parameters, namely the parasitic inductance of the diode L_p and the quality factor Q of the waveguide were used to fit the calculated tuning curve to the experimental data in Fig. 2. The quality factor Q is an intrinsic property of the tuner, and is defined [5] as the ratio of the energy stored to the energy dissipated per radian for a CPW section whose length is $l = m\lambda/4$ ($m = 1, 2, 3 \cdots$). The other electrical parameters of the diode were obtained from the manufacturer, and the rest of the parameters of the equivalent circuit were derived from low-frequency measurements of scale models. The best-fitting calculated tuning curve (Fig. 2) yielded the values $L_p = 0.04 \pm 0.01$ nH and $Q = 130 \pm 30$. Comparison of this value of Q with that obtained with other backshorts and tuning methods revealed that Q was limited by the ohmic conductor loss of the CPW section and that the contribution of the Mo backshort to ohmic losses was negligible. Therefore the laser tuning method did not negatively affect device performance as represented by Q. This effect comes about because of deep (>25 μm) penetration of the waves into the backshort, which arises from general considerations of boundary values and Maxwell's equations [6].

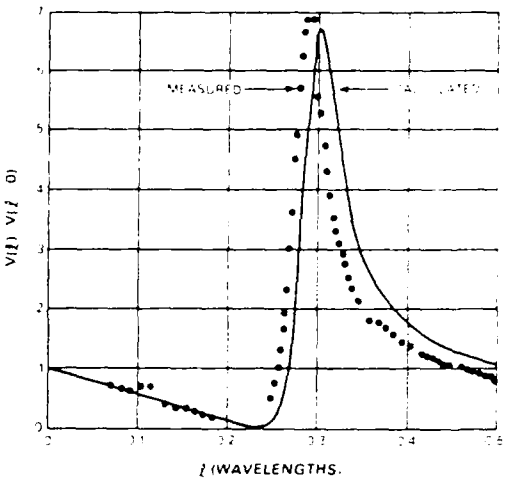

Fig. 2. The measured and calculated diode output $V(l)$ normalized to the output of an untuned circuit $V(l = 0)$, as a function of laser-etched tuner length l in units of guide wavelength λ at 33 GHz. The calculated best-fitting tuning curve was obtained with a value $Q = 130$. Note that the Q value is not degraded by the Mo backshort.

The advantages of laser tuning versus other techniques being explored such as solder and strip tuning [6] can be further understood as follows. An ideal tuner, when used to compensate for a shunt susceptance B, will have an admittance $Y_{tuner} = -jB$, and the total admittance seen by the circuit will be zero, resulting in maximum power transfer from the source to the load. In practice, $Y_{tuner} = -jB + j\Delta B_{tuner} + G_{tuner}$ where ΔB_{tuner} is an error arising from inaccuracy in backshort position and G_{tuner} is a conductance due to losses. The total admittance seen by the circuit is thus $j\Delta B_{tuner} + G_{tuner}$. It is clearly desirable to reduce both ΔB_{tuner} and G_{tuner}. G_{tuner} is directly related to Q and, as shown above, is insensitive to the Mo film. The magnitude of ΔB_{tuner}, on the other hand, is rapidly reduced with improved settability in backshort positioning Δl. In the solder and strip tuning methods $\Delta l \approx 32$ μm, with projected improvements to the 10-μm range. In contrast, the laser tuning had $\Delta l \approx 1$ μm with demonstrated [3] capabilities of $\Delta l \approx 0.25$ μm. This 1–2 orders of magnitude better settability and the accompanying reduced value of ΔB_{tuner} has a dramatic effect on the maximum power deliverable to the load.

Fig. 3 illustrates this improvement calculated for a simple circuit where the tuner is placed in shunt with a load (conductance G_{load}), a source (conductance G_{source}), and a parasitic element (susceptance B), and where $G_{load} = G_{source} = Y_0$, with Y_0 being the characteristic admittance of the tuner. P_{tuned} is the power delivered to the load when the tuner is used, and P_0 is the power delivered to the load with no tuner and with G_{source} chosen for maximum power transfer. In Fig. 3 the improvement in performance, P_{tuned}/P_0, due to tuning is plotted as a function of the parasitic susceptance B in units of Y_0, for the case where $f = 36$ GHz and $Q = 100$. It is evident from Fig. 3 that tuning with $\Delta l = 1$ μm (unoptimized laser tuning) is vastly superior to tuning with $\Delta l = 10$ μm (optimized solder or strip tuning). In particular, large improvements are achieved for $B/Y_0 \leq -10$. Similar results are obtained for other values of f and Q. In general, the larger the

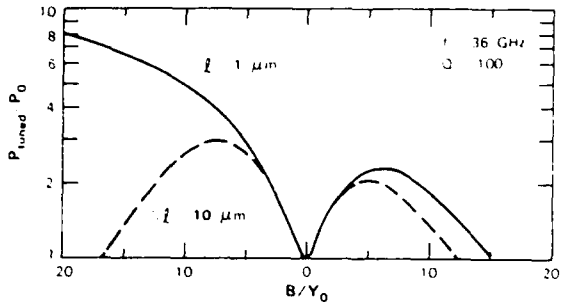

Fig. 3. Improvement in power output of the circuit, P_{tuned}/P_0, as a function of the parasitic susceptance B (in units of the characteristic admittance Y_0), for a model circuit with $G_{source} = G_{load} = Y_0$, operating at a frequency f = 36 GHz and tuner Q of 100. The two values of settability Δl correspond to the laser tuning (1 μm) and solder or strip tuning (10 μm) techniques. The desirability of a low value of Δl is evident.

f and the smaller the Q, the larger the range of $|B/Y_0|$ over which the Δl = 1-μm curve is significantly higher than that of Δl = 10 μm (see [6] and [7] for further details of the calculations).

In conclusion, we have demonstrated highly efficient *in situ* tuning of a millimeter-wave circuit with a commercial laser operating at visible wavelengths. The technique involves stepwise photochemical etching of a thin molybdenum film, which acts as a backshort in a coplanar waveguide tuner operating at 33 GHz. Straightforward application of the laser etching reaction in chlorine will permit adjustment of individual tuners in several minutes time. In these first experiments laser tuning to a settability of 1 μm, 10–30 times better than that of other tuning methods, was demonstrated without inducing any degradation in the Q of the waveguide.

Acknowledgment

The authors would like to thank J. G. Black for helpful discussions and K. Kundert for providing and modifying the circuit simulation tools used in this work.

References

[1] D. J. Ehrlich and J. Y. Tsao, "A review of laser microchemical processing," *J. Vac. Sci. Technol. B*, vol. 1, pp. 969–983, 1983.

[2] M. Rothschild, J. H. C. Sedlacek, and D. J. Ehrlich, "Laser photochemical etching of molybdenum and tungsten thin films by surface halogenation," *Appl. Phys. Lett.*, vol. 49, pp. 1554–1556, 1986.

[3] M. Rothschild, J. H. C. Sedlacek, J. G. Black, and D. J. Ehrlich, "Visible-laser photochemical etching of Cr, Mo and W," *J. Vac. Sci. Technol. B*, to be published, Jan. 1987.

[4] D. F. Williams and S. E. Schwarz, "A planar subharmonically-pumped 71 GHz receiver with integral feed antenna," *Int. J. Infrared and Millimeter Waves*, vol. 7, pp. 183–195, 1986.

[5] S. Ramo, J. R. Whinnery, and T. Van Duzer, *Fields and Waves in Communications Electronics*. New York: Wiley, 1984.

[6] D. F. Williams, J. H. C. Sedlacek, S. E. Schwarz, and D. J. Ehrlich, unpublished, 1986.

[7] D. F. Williams, "Millimeter-wave integrated circuit technology," Ph.D. dissertation, Univ. of Calif., Berkeley, July 1986.